Diffusion in Silicon

Written by: Scotten W. Jones

IC Knowledge LLC

Preface

The following document was written in 2000 as a chapter on Diffusion in Silicon for inclusion in a highly technical - text book on Silicon Integrated Circuit Process Technology. For marketing reasons we abandoned the book without completing it but this was one of several chapters that are complete. We have recently been posting chapters from this book for free download, we hope you find it useful. This particular chapter is an update of the previous diffusion chapter post and now includes the appendix with the properties of the error function.

Please note that this material was written back when we planned to publish it as a hard cover book in black and white and is not in color the way all of the current IC Knowledge reports are.

Scotten W Jones
President
IC Knowledge LLC
April 25, 2008

Contents

Diffusion in Silicon

1.1. Introduction

IC fabrication is accomplished by selectively changing the electrical properties of silicon through the introduction of impurities commonly referred to as dopants. In the early years of integrated circuit fabrication, deep semiconductor junctions required doping processes followed by a “drive-in” step to diffuse the dopants to the desired depth, i.e. diffusion was required to successfully fabricated devices. In modern state-of-the-art IC fabrication the required junction depths have become so shallow that dopants are introduced into the silicon at the desired depth by ion implantation and any diffusion of the dopants is unwanted, therefore diffusion has become a problem as opposed to an asset. There are many non state-of-the-art processes still in use throughout that industry where doping and diffusion are still in use and for state-of-the-art processes diffusion must be understood in order to minimize undesired effects. In this report the physical mechanisms of diffusion will be reviewed, the mathematics of diffusion will be presented and diffusion data will be provided to allow diffusion effects to be calculated.

1.2. Basic concepts

Throughout this report the concepts of impurity profile, background concentration and junction depth will be used.

- Impurity profile - the concentration of an impurity versus depth into the silicon.
- Background concentration - an impurity concentration existing in the silicon that an impurity profile is formed into.

- Junction depth - the depth at which the impurity profile concentration is equal to the background concentration.

Figure 1.1 illustrates the preceding three concepts. The impurity profile, C(x) varies with depth into the silicon, x, the background concentration C_B is shown at a constant level and the junction depth, x_j is the depth at which $C(x) = C_B$.

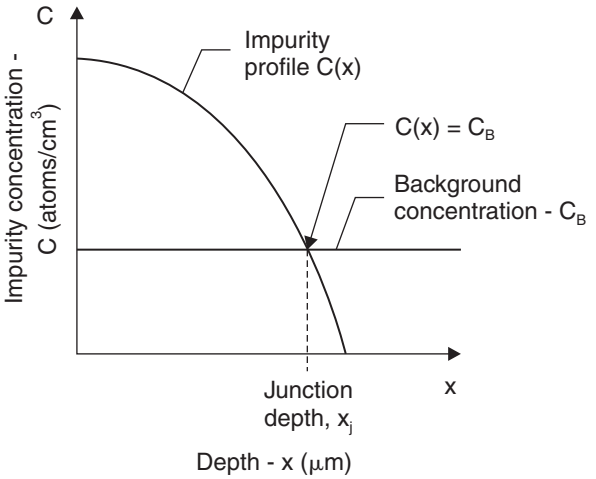

Figure 1.1: Impurity profile, background concentration and junction depth.

1.3. Atomic mechanisms of diffusion

Impurity atoms may occupy either substitutional or interstitial positions in the Si lattice (see figure 1.2). Impurity atoms utilized as dopants such as boron (B), phosphorus (P) and arsenic (As) occupy substitutional positions where the dopant atoms can contribute free electrons or holes to the silicon lattice (dopant atoms introduced to silicon by ion implantation may not occupy substitutional positions until the dopant is activated). During high temperature processing impurity profiles are redistributed through a process known as diffusion. The redistribution of impurities may be intentional as in a “drive-in” step or unintentional as a result of high temperature oxidation, deposition or annealing processes.

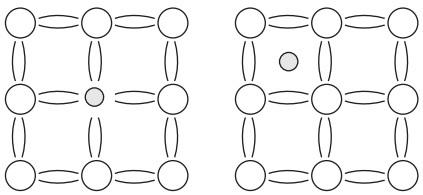

Figure 1.2: Substitutional and interstitial impurities in silicon.

- Diffusion - the redistribution of an initially localized substance throughout a background medium due to random thermal motion.

The movement of a substance due to diffusion is driven by the slope of the concentration profile.

Impurity atom diffusion may be vacancy, interstitial or a combination mechanism known as interstitialcy - see figure 1.3.

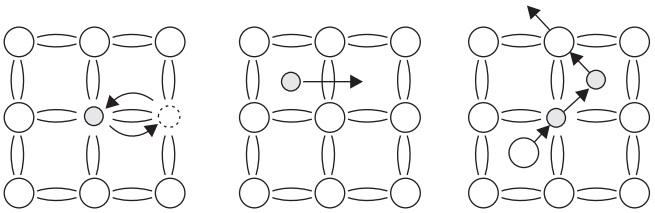

Figure 1.3: Vacancy, interstitial and interstitialcy diffusion mechanisms.

Vacancy diffusion occurs when a substitutional atom exchanges lattice positions with a vacancy - requires the presence of a vacancy. Interstitial diffusion occurs when an interstitial atom jumps to another interstitial position. Interstitialcy diffusion results from silicon self-interstitials displacing substitutional impurities to an interstitial position - requires the presence of silicon self-interstitials, the impurity interstitial may then knock a silicon lattice atom into a self-interstitial position. It is important to observe here that since dopant atoms such as phosphorus, arsenic and boron occupancy substitutional positions once activated, dopant diffusion is closely linked to and controlled by the presence of vacancy and interstitial point defects.

Whether an impurity atom occupies a substitutional or interstitial position in single crystal silicon, the atom is trapped in a periodic potential defined by the lattice - see figure 1.4. The probability of an atom jumping from one position to the next increases exponentially with increasing temperature.

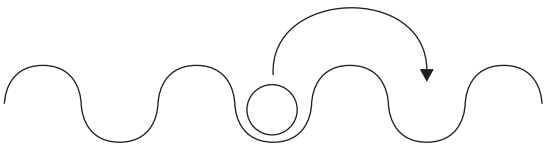

Figure 1.4: Impurity atom diffusing along a periodic potential.

In order to understand diffusion, consider the highly concentrated impurity profile illustrated in figure 1.5a, time = 0. If random thermal motion causes 20% of the atoms in each position to jump to a new position in each unit of time, 10% of the atoms would be expected to jump to the left and 10% of the atoms would be expected to jump to the right at time = 1. The areas of higher concentration would have more atoms jump out of the area than jump in. Over time the net result of the random thermal motion would be a gradual spreading of the profile - figure 1.5a, time = 0 to 1.5e, time = 4. At infinite time the impurity distribution would be uniform throughout the background medium

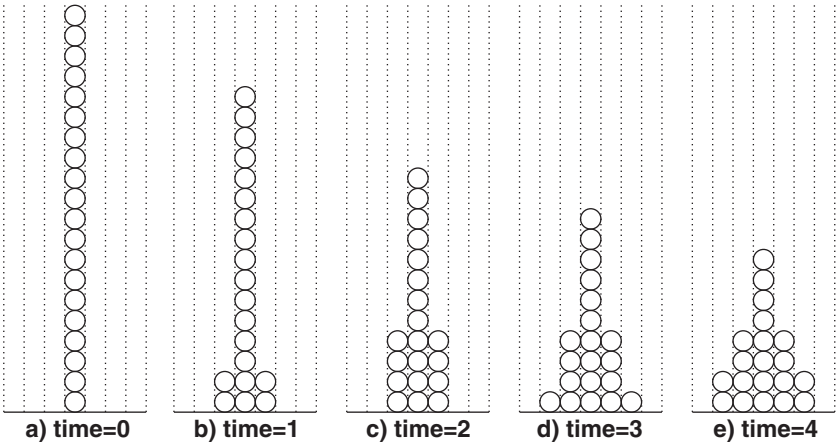

Figure 1.5: Impurity profile spreading due to random thermal motion - diffusion.

1.4. Mathematics of diffusion

From the basic principles outlined in the preceding section, the diffusion equations may be derived as follows [1],[2].

1.4.1. Fick's first law

Consider the two equal thickness slices of a solid illustrated in figure 1.6 where slice 1 and slice 2 have different impurity concentrations, C_1 and C_2 given by

$$C_1 = \frac{N_1}{A\lambda} \tag{1.1}$$

and

$$C_2 = \frac{N_2}{A\lambda} \tag{1.2}$$

and, N_1 and N_2 are the number of impurity atoms in slice 1 and slice 2 respectively, A is the cross sectional area of the slices and λ is the thickness of the slices.

Atoms throughout the solid are constantly vibrating from thermal energy. At a given temperature each atom in the slice has a frequency of jumps to the adjacent slice, ν, with equal probability of jumping in either direction, therefore the frequency of jumps from one slice to the next in a particular direction is $\nu/2$. For the plane separating slice 1 from slice 2, the flow of atoms across the boundary is

$$\frac{+\Delta N_{1->2}}{\Delta t} = \frac{N_1 \nu}{2} \tag{1.3}$$

and

$$\frac{-\Delta N_{2->1}}{\Delta t} = \frac{N_2 \nu}{2} \tag{1.4}$$

where t is time. Note that left to right is the positive direction and right to left is the negative direction of motion.

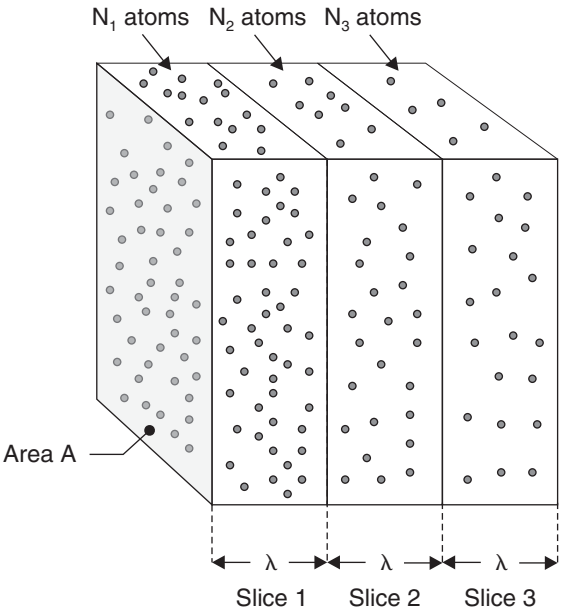

Figure 1.6: Diffusion from a concentration gradient.

Combining equations 1.3 and 1.4 yields the net flow across the boundary

$$\frac{\Delta N}{\Delta t} = \frac{\nu}{2}(N_1 - N_2) \tag{1.5}$$

and substituting concentration from equations 1.1 and 1.2 into equation 1.5, gives

$$\frac{\Delta C}{\Delta t} = \frac{(C_1 - C_2)A\lambda\nu}{2} \tag{1.6}$$

Since the concentration gradient is given by

$$\frac{\Delta C}{\Delta x} = \frac{C_2 - C_1}{\lambda} \tag{1.7}$$

equation 1.6 and 1.7 can be combined to give

$$\frac{\Delta C}{\Delta t} = \frac{-A\lambda 2\nu}{2}\frac{\Delta C}{\Delta x} \tag{1.8}$$

By now introducing flux, j, defined as

- Flux - the number of units passing through a boundary area per unit time.

and dividing equation 1.8 by area, the expression for flux may be found as

$$j = \frac{1}{A}\frac{\Delta C}{\Delta t} = -\frac{\lambda^2 \nu}{2}\frac{\Delta C}{\Delta x} \tag{1.9}$$

The diffusion constant D, is now introduced and defined as

$$D \equiv \frac{\lambda^2 \nu}{2} \tag{1.10}$$

Combining equations 1.9 and 1.10 results in

$$j = -D\frac{\Delta C}{\Delta x} \tag{1.11}$$

which in partial differential terms is known as Fick's first law

$$j = -D\frac{\partial C}{\partial x} \tag{1.12}$$

Fick's first law relates the flux of atoms across a boundary to the concentration gradient and from Fick's law it can be seen that regions with a large concentration gradient diffuse more rapidly than regions with a small concentration gradient.

1.4.2. Fick's second law

Fick's first law allows the diffusive flux as a function of the concentration gradient to be calculated, Fick's second law allows the concentration function, C(x), to be calculated as a function of time.

Consider the second slice in figure 1.5. Since matter is conserved the time change in concentration in slice 2 must be the sum of the fluxes across the slice 1 to slice 2 boundary and the slice 2 to slice 3 boundary.

Which results in

$$\frac{\Delta C}{\Delta t} = j_1 - j_2 \tag{1.13}$$

and

$$\frac{j_1 - j_2}{\lambda} = \frac{\Delta j}{\Delta x} \tag{1.14}$$

therefore

$$\frac{\Delta C}{\Delta t} = -\frac{\Delta j}{\Delta x} \tag{1.15}$$

In differential terms, equation 1.15 is the transport equation

$$\frac{\partial C}{\partial t} = -\frac{\partial j}{\partial x} \tag{1.16}$$

Substituting Fick's first law - equation 1.12 into equation 1.16 gives Fick's second law

$$\frac{\partial C}{\partial t} = D\frac{\partial^2 C}{\partial x^2} \tag{1.17}$$

Fick's second law as derived in the preceding sections is identical in form to the equation for heat conduction differing only in the constant D, and therefore the large body of work on heat flow can be applied to the problems of impurity atom diffusion in silicon.

1.5. Diffusion equations

Fick's laws can now be applied to solve diffusion problems of interest. As was the case previously the solutions presented here assume a constant diffusivity.

1.5.1. Infinite source diffusion into a semi-infinite body - single step diffusion

Early in the development of integrated circuit fabrication technology, semiconductor doping was accomplished by exposing semiconductor substrates to a high concentration of the desired impurity. In order to maintain good process control, the concentration of the impurity dopant was maintained at a level in excess of the level required to achieve solid solubility of the dopant at the semiconductor surface (solid solubility is the maximum doping level that is soluble in silicon at a given temperature - see section 1.7). The high concentration of dopant reduced the process control requirements to time and temperature. The doping source may be a gas containing the dopant of interest such as arsine - AsH_3 - an arsenic source, or a glass layer such as P_2O_5 as a phosphorus source. The dopant in these cases may be considered an infinite impurity source in contact with a semi-infinite medium (the semiconductor substrate thickness is orders of magnitude greater than the diffusion depth of the dopant for most instances of practical interest). The surface concentration of the semiconductor will be C_S set by the solid solubility at any time during the diffusion process and the dopant concentration in the gas C_G is > C_S - see figure 1.7

To solve for the impurity profile in the silicon versus time, Fick's second law - equation 1.17, must be solved for the boundary and initial conditions, where the boundary conditions are given by

$$C = C_0, \quad x = 0, \quad t > 0 \tag{1.18}$$

and the initial conditions are

$$C = 0, \quad x > 0, \quad t = 0 \tag{1.19}$$

.

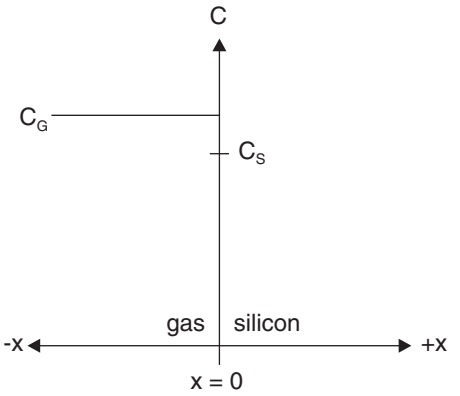

Figure 1.7: Single step diffusion - initial conditions.

The solution to Fick's law for single step diffusion that will be derived here will apply Laplace transforms after reference [4]. There are several alternate methods that can also be utilized to reach the same result. The laplace transform for a known function of t, for t > 0, is

$$\bar{f}(p) = \int_0^\infty e^{-pt} f(t)dt \tag{1.20}$$

Laplace transforms of common functions may be constructed by integrating equation 1.20.

Starting with Fick's law - equation 1.17, multiplying both sides by e^{-pt} and integrating with respect to t from zero to infinity results in

$$\int_0^\infty e^{-pt} \frac{\partial^2 C}{\partial x^2} dt - \frac{1}{D}\int_0^\infty e^{-pt} \frac{\partial C}{\partial t} dt = 0 \tag{1.21}$$

Assuming that the orders of differentiation and integration can be interchanged (this can be justified for the functions of interest [4]), then

$$\int_0^\infty e^{-pt} \frac{\partial^2 C}{\partial x^2} dt = \frac{\partial^2}{\partial x^2} \int_0^\infty C e^{-pt} dt = \frac{\partial^2 \bar{C}}{\partial x^2} \tag{1.22}$$

Integrating by parts

$$\int_0^\infty e^{-pt} \frac{\partial C}{\partial t} dt = [Ce^{-pt}]_0^\infty + p\int_0^\infty Ce^{-pt} dt = p\bar{C} \tag{1.23}$$

Since the term in the square brackets vanishes at t = 0 for the initial conditions - equation 1.19 and at t = infinity through the exponential factor - equation 1.17 reduces to

$$D\frac{\partial^2 \overline{C}}{\partial x^2} = p\overline{C} \tag{1.24}$$

By treating the boundary conditions - equation 1.18 in the same way

$$\overline{C} = \int_0^\infty C_0 e^{-pt} dt = \frac{C_S}{p}, \quad x = 0 \tag{1.25}$$

Thus the Laplace transform reduces from the partial differential equation 7.17 to an ordinary differential equation 1.24.

The solution of equation 1.24 that satisfies equation 1.25 and for which C bar remains finite as x approaches infinity is

$$\overline{C} = \frac{C_S}{p} e^{-bx} \tag{1.26}$$

where, $b^2 = p/D$. The Laplace transform for equation 1.26 is [4]

$$C(x, t) = C_S \, erfc \, \frac{x}{2\sqrt{Dt}} \tag{1.27}$$

where, erfc is the complementary error function, one of the most important functions in diffusion theory. Error function properties are presented in appendix F.

The concentration of impurities versus depth into the silicon calculated using equation 7.27 is plotted as a linear plot versus 2 multiplied by the square root of DT in the top of figure 7.8 and as a log plot versus 2 root DT in the bottom of figure 1.8.

The total number of impurity atoms Q which enter a 1 cm^2 section of silicon is defined by

$$Q(t) \equiv \int_0^\infty C(x, t) dx \tag{1.28}$$

Integrating equation 1.28 results in

$$Q(t) = \frac{2}{\sqrt{\pi}} \sqrt{Dt} C_S \tag{1.29}$$

If a single step diffusion as outlined above is used to introduce impurities into silicon as dopants, equation 1.29 can be utilized to calculate the total number of dopant atoms introduced. Q will also be used later to calculate profiles resulting from two step diffusion processes.

The gradient or slope of the impurity profile can be calculated by

$$\left.\frac{\partial C}{\partial x}\right|_{(x, t)} = -\frac{C_S}{\sqrt{\pi Dt}} e^{-x^2/4Dt} \tag{1.30}$$

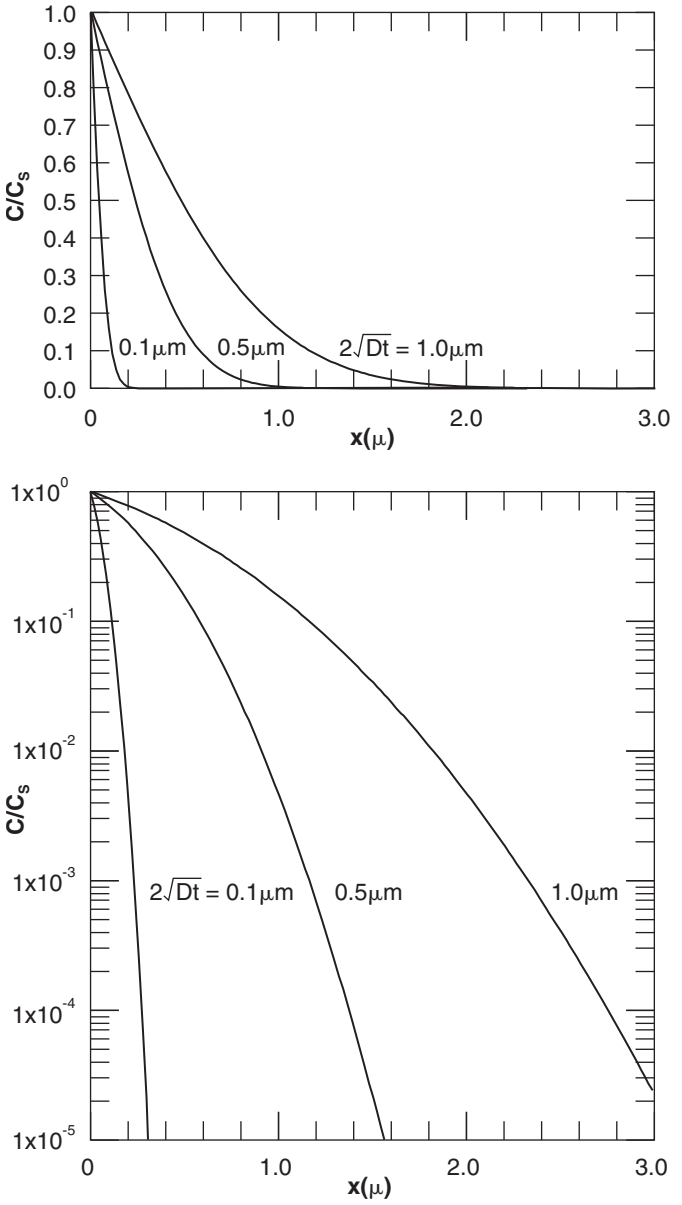

Figure 1.8: Complementary error function profile evolution versus time [5].

Using the asymptotic approximation for the complementary error function from appendix F, equation 1.31 results that is valid for most practical situations [5].

$$\left.\frac{\partial C}{\partial x}\right|_{(x,\,t)} \cong -\frac{x}{2Dt}C(x,t) \tag{1.31}$$

1.5.2. Plane source - two step diffusion

When a single step diffusion is used to introduce dopant into a semiconductor, a follow-on second drive-in diffusion is also frequently used. During deposition an oxide-masking layer maybe used to mask the dopant from some areas of the semiconductor. If single step diffusion is performed with a long cycle, the dopant can diffuse through the masking oxide resulting in a loss of the desired pattern. Alternately a short single step diffusion can be used to introduce the desired Q or total dopant into the semiconductor. The single step diffusion is followed by an etch back to remove the doped portion of the oxide and then a long drive-in cycle can be used without fear of the dopant penetrating the masking oxide. Figure 1.9 illustrates the pre-deposition and drive in doping process.

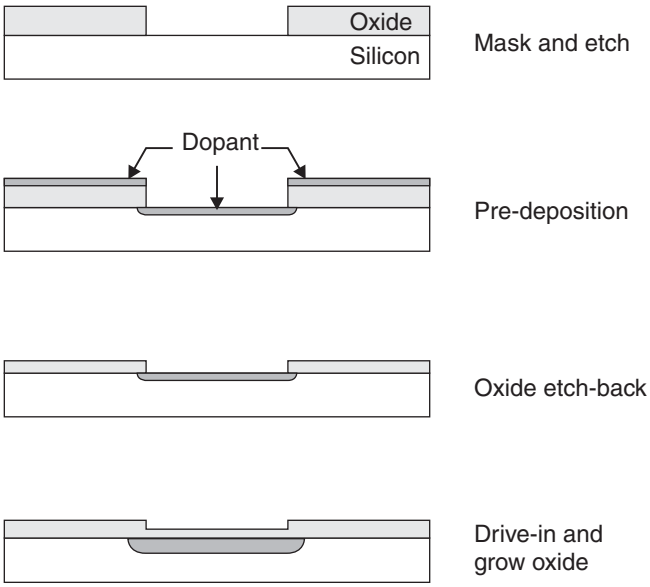

Figure 1.9: Pre-deposition and drive-in process.

Following the pre-deposition step the impurity distribution can be determined by solving the diffusion equation which satisfies the boundary conditions

$$\left.\frac{\partial C}{\partial x}\right|_{(0,\,t)} = 0 \tag{1.32}$$

and

$$C(\infty, t) = 0 \tag{1.33}$$

The solution must also provide for a constant Q to be maintained in the semiconductor. The initial condition is given by equation 1.27 using the Dt for the pre-deposition step. Solving equation 1.27 with the boundary condition given by equation 1.32 and equation 1.33 is a difficult problem. In practice the Dt from the drive-in step is much greater than the Dt for the pre-

deposition step. A practical approximation is to assume that the total dopant Q is located in a sheet at the interface.

By differentiation it may be shown that

$$C = \frac{A}{\sqrt{t}} e^{-x^2/4Dt} \tag{1.34}$$

is a solution to equation 1.17 where A is an arbitrary constant. Equation 1.34 is symmetric about x, tends to zero as x approaches infinity positively or negatively for t>0, and at t=0 vanishes everywhere but x=0, where it becomes infinite.

The total amount of impurities Q, diffusing in a cylinder of infinite length and unit cross section is given by

$$Q = \int_{-\infty}^{\infty} C dx \tag{1.35}$$

If the concentration distribution is given by equation 1.34, then

$$x^2/4Dt = \xi^2, \quad \mathrm{dx} = 2\sqrt{Dt}\, d\xi \tag{1.36}$$

and

$$Q = 2A\sqrt{D} \int_{-\infty}^{\infty} e^{-\xi^2} d\xi = 2A\sqrt{\pi D} \tag{1.37}$$

Equation 1.37 shows that amount of impurity diffusing remains a constant and is equal to the amount in the interface sheet at x=0. Therefore, substituting for A from equation 1.37 into equation 1.34 results in

$$C(x, t) = \frac{Q}{2\sqrt{\pi Dt}} e^{-x^2/4Dt} \tag{1.38}$$

In the actual pre-deposition - drive-in case being considered the gas-silicon interface truncates one side of the distribution, (equation 1.35 assumes the distribution is continuous in both directions). Equation 1.38 becomes

$$C(x, t) = \frac{Q}{\sqrt{\pi Dt}} e^{-x^2/4Dt} \tag{1.39}$$

Which is the drive-in concentration following pre-deposition. Equation 1.39 is the well known gaussian distribution. The top of figure 1.10 illustrates the progression of the impurity profile with time as a linear plot and the bottom of figure 1.10 illustrates a log plot.

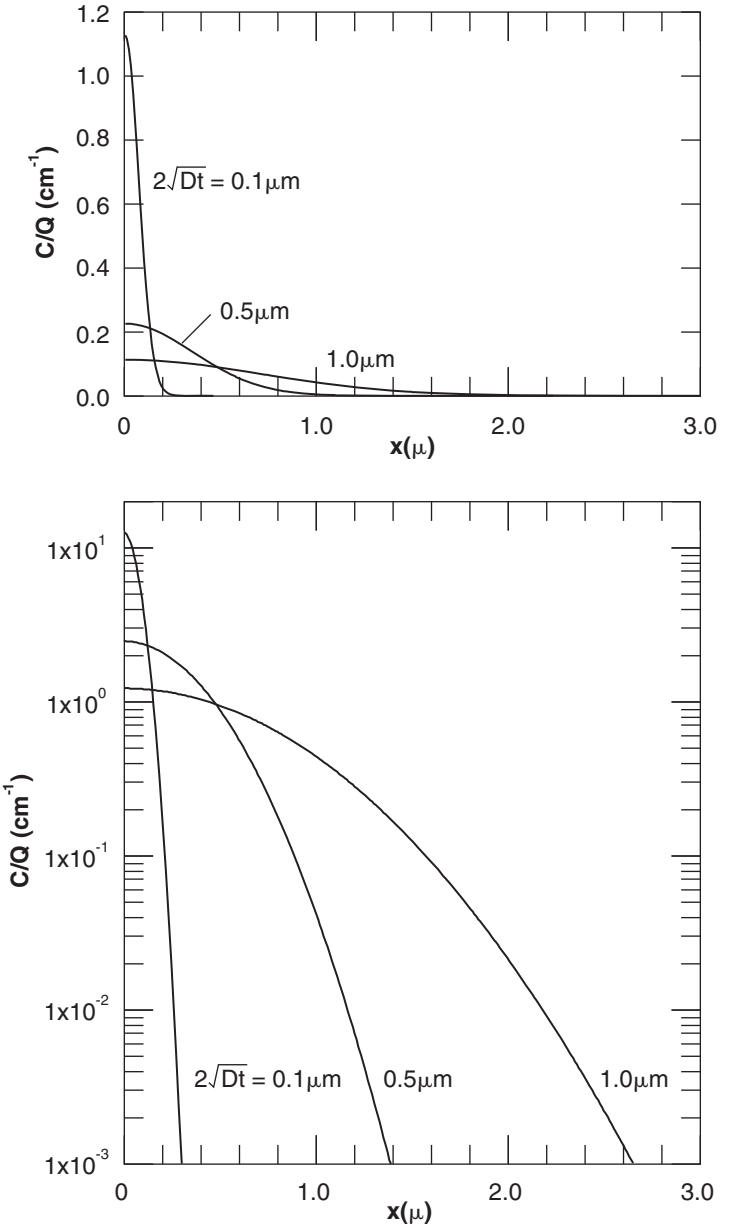

Figure 1.10: Gaussian distribution normalized concentration versus distance for successive times [5].

Since Q is fixed, as the impurities diffuse into the silicon the surface concentration C_S must decrease - this is in contrast to the single step diffusion case where C_S is a constant. From equation 1.39, the surface concentration may be calculated by

$$C_S(t) = \frac{Q}{\sqrt{\pi Dt}} \tag{1.40}$$

Thus the concentration distribution can also be represented by

$$C(x, t) = C_S(t)e^{-x^2/4Dt} \tag{1.41}$$

The gradient of the concentration distribution can be obtained by differentiating equation 1.41 and is given by

$$\left.\frac{\partial C}{\partial x}\right|_{(x, t)} = -\frac{x}{2Dt}C(x, t) \tag{1.42}$$

Figure 1.11 presents some values of the error function and Gaussian function versus z where

$$z = \frac{x}{2\sqrt{Dt}} \tag{1.43}$$

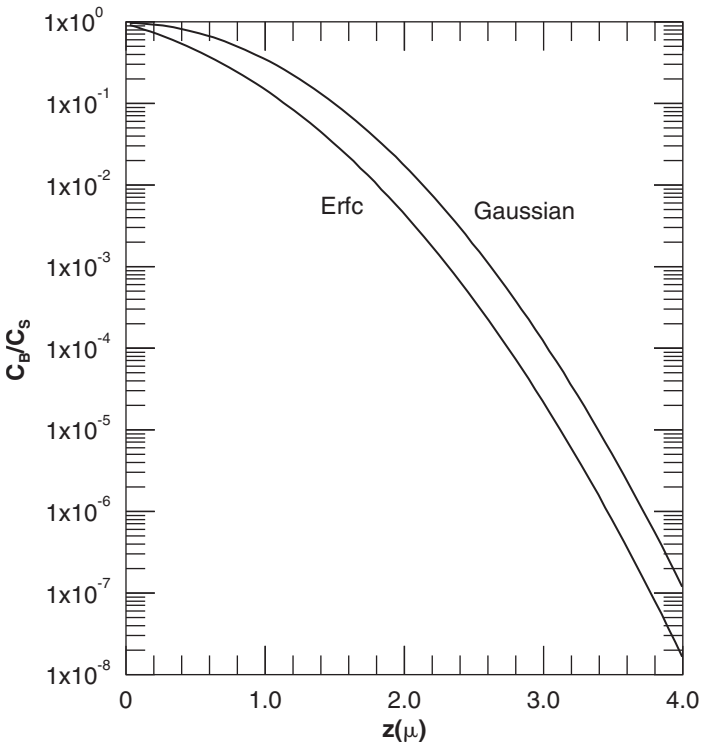

Figure 1.11: Gaussian and error function values versus z.

As will be seen in the problem section, figure 1.11 is very useful for performing diffusion calculations.

1.6. Diffusivity

In equation 1.10 the concept of a diffusion constant - the diffusivity was introduced. In this section the physical basis of diffusivity will be reviewed and some data on diffusivity values will be presented.

In order for an impurity to diffuse through silicon, the impurity must either move around silicon atoms or displace silicon atoms. During interstitial diffusion the diffusing atom jumps from one interstitial position to another interstitial position, with relatively low barrier energy and a relatively high number of interstitial sites. Substitutional atoms require the presence of a vacancy or an interstitial to diffuse and must break lattice bonds. Vacancy and interstitial formation are relatively high-energy processes and so are relatively rare in equilibrium (as will be seen later certain processes can result in concentrations of interstitials and or vacancies well in excess of equilibrium). Breaking bonds to the lattice is also a relatively high-energy process and substitutional atoms tend to diffuse at a much lower rate than interstitial atoms.

The diffusion process can be characterized by a barrier with activation energy E_a, where E_a is the energy required to jump from one site to the next site. The probability of an atom jumping to another site is given by the product of two terms. The first term is the frequency with which the atom collides with the barrier ν_0 (the frequency of atomic oscillation in silicon is approximately 10^{13} to 10^{14} /sec.). The second term is the probability the atom will surmount the barrier during a collision (given by the boltzman factor $\exp(-E_a/kT)$) where k is boltzman's constant and T is the temperature in degrees Kelvin. The rate at which atoms jump to a new position is given by

$$\nu = \nu_0 e^{-E_a/kT} \tag{1.44}$$

Each atom can move to any adjacent site, so equation 1.44 should be multiplied by the number of adjacent sites which is four for silicon for both the interstitial and substitutional case. For the interstitial case equation 1.44 becomes

$$\nu_{inst} = 4\nu_0 e^{-E_a/kT} \tag{1.45}$$

For substitutional atoms an additional term must be added to account for the probability of a vacancy or interstitial existing in the adjacent site (vacancies for vacancy diffusion and interstitials for interstitialcy diffusion). If E_d is the energy for point defect formation, the resulting expression is

$$\nu_{subst} = 4\nu_0 e^{-(E_a + E_d)/kT} \tag{1.46}$$

Experimentally determined activation energies for interstitial atoms are approximately 0.5eV and for substitutional atoms are approximately 3eV (including defect formation) [3]. It is

now possible to rewrite the diffusion constant equation 1.10 in terms of the physical properties of the materials.

Substituting equation 1.45 into equation 1.10 and taking into account that the spacing between atoms λ is d divided by the square root of 3 for a diamond structure, interstitial diffusivity is given by

$$D = \frac{4\nu_0 d^2}{6} e^{-E_a/kT} \tag{1.47}$$

Substituting equation 1.46 into equation 1.10 and taking into account the inter-atomic spacing gives the diffusivity for substitutional atoms of

$$D = \frac{4\nu_0 d^2}{6} e^{-(E_a + E_d)/kT} \tag{1.48}$$

Equations 1.47 and 1.48 imply that the diffusivity for all interstitial atoms will be the same and the diffusivity for all substitutional atoms will be the same, this is not the case. Electric fields, impurity - lattice size mis-match induced strain and multiple diffusion mechanisms complicate actual diffusivity values.

From the discussion of diffusion mechanisms presented in section 1.2 one would expect that vacancy diffusion would depend on vacancy concentration, which is a function of temperature, and any non-equilibrium vacancy generation or annihilation mechanisms. Conversely, interstitialcy diffusion would be expected to be sensitive to silicon self-interstitial concentration which, also depend on temperature and non-equilibrium processes. There are a number of IC fabrication processes which can generate non-equilibrium point defect concentrations. Table 1.1 summarizes process effects on point defects where V indicates vacancy generation and I indicates interstitial generation.

Table 1.1: Process generated point defects

Process step	Point defects
Ion implantation	I-V pairs
Oxidation	I
Nitridation	V
Salicidation	V

Ion implantation generates interstitial vacancy pairs by knocking lattice atoms from their lattice position, oxidation is a partially complete reaction and injects interstitials into the underlying silicon, nitridation and silicide formation inject vacancies. Silicon surfaces act as recombination sites for point defect concentrations so that the proximity of a surface must be taken into account. Interstitials may also cluster together to form defects which grow and shrink depending on time, temperature and interstitial concentrations with the result that defects may act as an interstitial sink or source. Interstitials and vacancies may also recombine in the bulk.

In order to accurately calculate diffusivity it is therefore important to understand the atomic mechanism by which each dopant diffuses as well as the local point defect concentrations. Effective diffusivities in the presence of point defects can be expressed as

$$\frac{D_{eff}}{D^*} = f_I \frac{C_I}{C^*_I} + (1 - f_I) \frac{C_V}{C^*_V} \tag{1.49}$$

where, D_{eff} is the effective diffusivity, D^* is the equilibrium diffusivity, f_I is the fraction of diffusion due to an interstitialcy mechanism, C_I is the interstitial concentration, C^*_I is the equilibrium interstitial concentration, C_V is the vacancy concentration and C^*_V is the equilibrium vacancy concentration.

Equation 1.49 allows vacancy, interstitialcy or mixed vacancy-interstitialcy diffusivity in the presence of point defects to be modeled.

One of the classic experiments for determining the effect of interstitials on diffusivity and therefore the interstitialcy component of diffusion is illustrated in figure 7.12. The experiment begins with the formation of a uniform doped layer. A layer of silicon nitride (Si_3N_4) is then deposited and patterned to leave an opening where oxidation is to take place - Si_3N_4 of sufficient thickness can block thermal oxidation. A silicon dioxide (SiO_2) layer is then grown in the Si_3N_4 opening. Oxidation is usually incomplete and approximately 1 in every 1,000 silicon atoms are un-reacted. The un-reacted silicon atoms breaks free of the interface and becomes silicon self-interstitials. The concentration of silicon self-interstitials is higher under the center region where oxidation is occurring and if interstitials increase the diffusivity of the dopant being measured then the dopant will diffuse deeper under the center section. Conversely if interstitials retard diffusion, for example if interstitials recombine with vacancies limiting the vacancy supply for vacancy diffusion, the dopant will diffuse to a shallower depth under the center section.

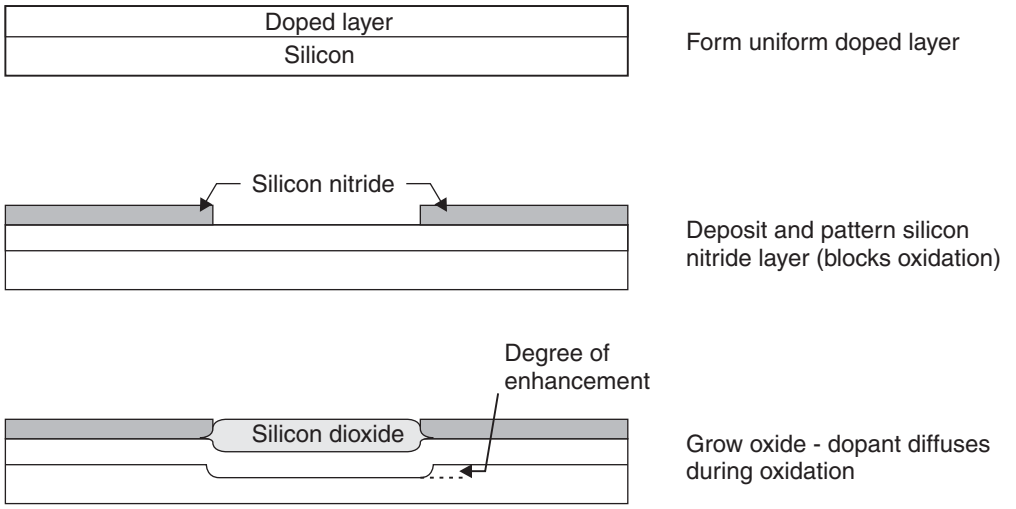

Figure 1.12: Experiment to measure oxidation enhanced diffusion.

It is important to note here that the oxidation reaction is consuming silicon in the center section. Without diffusivity enhancement the distance between the SiO_2 - Si interface and diffusion boundary under the center section would be smaller than the distance between the Si_3N_4 - Si interface and the diffusion boundary out at either side.

Many researchers have investigated the mechanisms of diffusion. Table 1.2 summarizes the interstitialcy component

Table 1.2: Interstitialcy component of diffusion [20].

Element	Temperature (°C)				Reference
	950	1,000	1,050	1,100	
Aluminum				0.6-0.7	11
Antimony				0.02	9
				0.02	11
Arsenic	0.10	0.12	0.15	0.19	12
				0.2-0.4	9
	0.22	0.25	0.30	0.35	19
	0.09	0.09	0.09	0.09	8
	0.25	0.30	0.35	0.42	10
				0.2-0.5	11
Boron	0.16	0.17	0.18	0.19	12
		0.24-			9
	0.22	0.34	0.42	0.52	19
	0.17	0.32	0.17	0.17	8
	0.38	0.17	0.60	0.80	10
		0.45		0.8-1.0	11
Gallium				0.6-0.7	11
Indium		0.30			9
Phosphorus	0.14	0.16	0.19	0.23	12
		0.38		0.55	9
	0.27	0.34	0.42	0.51	19
	0.12	0.12	0.12	0.12	8
	0.30	0.35	0.45	0.55	10
				0.5-1.0	11

From table 1.2 it is clear that there is a great deal of disagreement about the interstitialcy component of diffusion. Recently Grossman [67] has pointed out that experimental measurements of the interstitialcy component of diffusion for a single species require the solution to a single equation, equation 1.49 with three unknowns, the percent of interstitialcy diffusion and the ratios of interstitial and vacancy concentrations to equilibrium. If however, two different

diffusing species are measured under identical conditions a system of two equation in two unknowns can be formulated and solved without resulting to assumptions about the vacancy and interstitial ratios. Grossman has performed this experiment for boron and antimony and found

$$f_B(860^oC) \geq 0.98 \mp 0.01 \tag{1.50}$$

and

$$f_{Sb}(790^oC) \leq 0.01 \mp 0.01 \tag{1.51}$$

Or in other words, B diffuses through an almost exclusively interstitialcy mechanism and Sb diffuses through an almost exclusively vacancy mechanism. Grossman further suggests that any substitutional dopant in silicon should diffuse through either a pure vacancy or a pure interstitialcy mechanism.

A complete diffusion model needs to account for point defect interactions with the diffusing species and also formations of defect clusters. For example, a complete set of interactions for boron would need to account for the following eight interactions [68]:

A neutral interstitial interacts with a cluster to either grow or shrink the cluster

$$I^0 + C \leftrightarrow C \tag{1.52}$$

An interstitial and vacancy either annihilate each other or are generated as a Frenkel pair

$$I^0 + V^0 \leftrightarrow 0 \tag{1.53}$$

An interstitial and a hole interact to create a positively charged interstitial from a neutral interstitial or a positively charged interstitial releases a hole and becomes neutral.

$$I^0 + h^+ \leftrightarrow I^+ \tag{1.54}$$

A negatively charged boron atom combines with a neutral interstitial to form a neutral boron - interstitial pair and release an electron or a neutral boron - interstitial pair captures an electron and breaks up into a negatively charged boron atom and a neutral interstitial.

$$B^- + I^0 \leftrightarrow BI^0 + e^- \tag{1.55}$$

A negatively charged boron atom combines with a neutral interstitial and a hole to form a neutral boron - interstitial pair or a natural boron - interstitial pair releases a hole and breaks up into a negatively charged boron atom and a neutral interstitial.

$$B^- + I^0 + h^+ \leftrightarrow BI \tag{1.56}$$

A neutral boron - interstitial pair combine with a vacancy annihilating the vacancy - interstitial pair and releasing a negatively charged boron atom and a hole or a hole and a negatively charged boron atom combine and generate a neutral boron - interstitial pair and release a vacncy.

$$BI^0 + V^0 \leftrightarrow B^- + h^+ \tag{1.57}$$

A positively charged boron - interstitial pair combine with a vacancy annihilating the vacancy - interstitial pair and releasing a negatively charged boron atom and two holes or two holes and a negatively charged boron atom combine and generate a positively charged boron - interstitial pair and release a vacancy.

$$BI^+ + V^0 \leftrightarrow B^- + 2h^+ \tag{1.58}$$

A negatively charged boron atom and a positively charged boron - interstitial pair combine to form a neutral boron cluster or a neutral boron cluster breaks apart into a negatively charged boron atom and a positively charged boron - interstitial pair.

$$B^- + BI^+ \leftrightarrow BB_{cls} \tag{1.59}$$

The equation set can be implemented through a set of reaction diffusion equations of the form [69]:

$$\frac{\partial C_{BI^0}}{\partial t} = \frac{\partial}{\partial x}\left[D_{BI^0} \cdot \frac{\partial C_{BI^0}}{\partial x}\right] + K_F^1 C_B - C_{I^0} - K_R^1 C_{BI^0} n^- - K_F^2 C_{BI} + C_{V^0} + K_R^2 C_B - p \tag{1.60}$$

This system of equation contains a large number of parameters that must be know in order to evaluate the model predictions. Recently general purpose differential equation solvers have become available which allows systems like this to be evaluated [80]. It seems reasonable to expect that commercial process simulators will include such models in the future.

In order to enable the reader to make diffusion calculations of reasonable accuracy Fair's diffusivity model will be presented in the next few sections. Fair has developed a model for diffusivity based on impurity interactions with charged vacancy states that provides a reasonably good fit to most observed diffusion results [6],[7]. Fair's model calculates diffusivity as the sum of the individual charged vacancy - impurity diffusivities.

The intrinsic model is given by

$$D_i = D^0 + D^+ + D^- + D^= + \ldots \quad \text{for n or p} << n_i \tag{1.61}$$

where: D_i is the intrinsic diffusivity, D^0 is the neutral vacancy - impurity diffusion, D^+ is the positively charged vacancy - impurity diffusion, D^- is the negatively charged vacancy - impurity diffusion and $D^=$ is the doubly negatively charged vacancy - impurity diffusivity and n_i is the intrinsic carrier concentration - see chapter 1.

For extrinsic silicon

$$D_x = D^0 + D^+\left[\frac{p}{n_i}\right] + D^-\left[\frac{n}{n_i}\right] + D^=\left[\frac{n}{n_i}\right]^2 + \ldots \quad \text{for n or p} >> n_i \tag{1.62}$$

where, D_x is the extrinsic diffusivity. For specific impurities not all vacancy charge state - impurity combinations will participate in the diffusivity.

Even though it is now known that substitutional diffusion is not strictly vacancy dominated, Fair's model is useful for the reasonable results it obtains without resorting to complex simulation.

The temperature dependence of the diffusivity values presented in the next several sections will take the arhenius form

$$D = D_0 e^{-E_a/kT} \tag{1.63}$$

where D_0 is a pre exponential constant.

Arhenius equations form a straight line when ln(D) is plotted versus 1/T.

1.6.1. Diffusivity of antimony in silicon

Antimony is believed to diffuse by a purely vacancy mechanism with the Sb^+V^- dominating. The intrinsic diffusivity of antimony is given by [6]

$$D_i = 0.214 e^{-3.65/kT} \quad \text{cm}^2/\text{s} \tag{1.64}$$

The extrinsic diffusivity of antimony is given by [6]

$$D_x = D^0 + D^- \left[\frac{n}{n_i}\right] \tag{1.65}$$

and D^+ and $D^= = 0$, D^0 and D^- are given by

$$D^0 = 0.214 e^{-3.65/kT} \quad \text{cm}^2/\text{s} \tag{1.66}$$

and

$$D^- = 15.0 e^{-4.08/kT} \quad \text{cm}^2/\text{s} \tag{1.67}$$

The diffusivity of antimony versus temperature is illustrated in figure 1.13

Antimony has a large tetrahedral radius of 0.136nms versus a radius of 0.118nms for silicon giving a 1.15 mismatch factor and creating strain in the silicon lattice [3]. Antimony diffusion is retarded by oxidation due to injected silicon self-interstitials annihilating vacancies. Table 1.3 presents the ratio of antimony diffusivity under oxidizing (dry O_2)and non-oxidizing conditions for a variety of times and temperatures [71].

Table 1.3: Oxidation retardation of antimony diffusivity [71]

Temperature (^{o}C)	Time (mins.)	D_{OX}/D^*
1,000	500	0.20
1,000	1,500	0.18
1,100	10	0.25
1,100	60	0.30
1,100	600	0.44

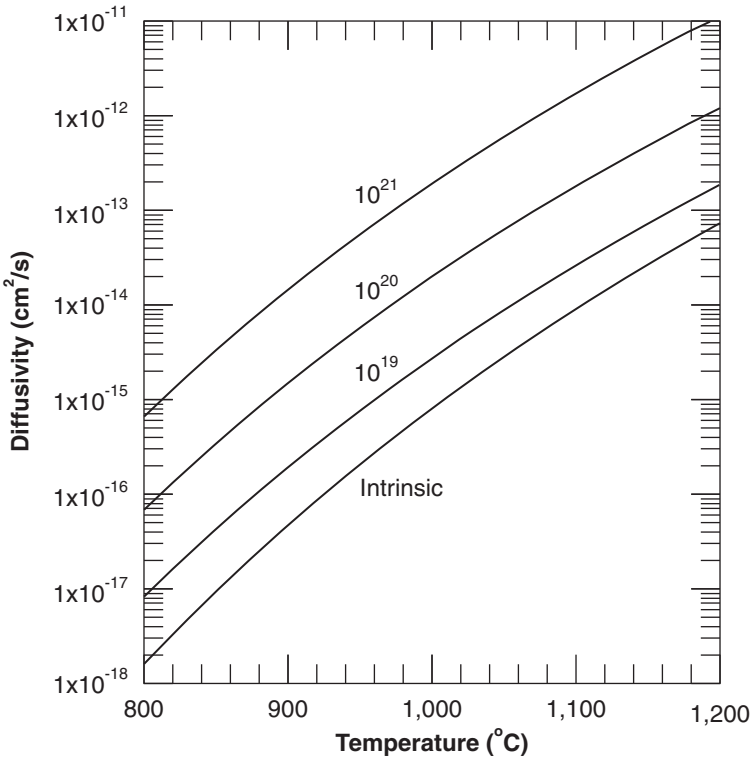

Figure 1.13: Diffusivity of antimony in silicon versus temperature and antimony concentration. Calculated from equations 1.64 through 1.67.

1.6.2. Diffusivity of arsenic in silicon

Arsenic is believed to diffuse primarily through a vacancy mechanism with an interstitialcy component [7]. Estimates of the interstitialcy component of arsenic diffusion are presented in table 1.2. The arsenic interstitial formation energy is estimated to be a relatively high 2.5eV. Above approximately 1,050°C diffusion is dominated by $As^{+}V^{-}$ vacancy pairs with $As^{+}V^{=}$ being relatively rare due to the small pair binding energy. Oxidation has little effect on arsenic diffusivity due to the high arsenic interstitial formation energy.

The intrinsic diffusivity of arsenic is given by [6]

$$D_i = 22.9e^{-4.1/kT} \quad \text{cm}^2/s \tag{1.68}$$

At high concentration (>10^{20} atoms/cm^3) arsenic diffusivity is complicated by clustering. Arsenic atoms are believed to form clusters where 3 arsenic atoms bond with an electron (see section 1.7 - solid solubility). Clusters are virtually immobile at T <1,000°C. Below 1,000°C equations 7.68 through equation 1.71 gives the diffusivity for un-clustered arsenic. Above ~1,000°C arsenic un-clusters and equation 1.68 through equation 1.71 again gives the diffusivity

$$D_x = D^0 + D^- \left[\frac{n}{n_i}\right] \tag{1.69}$$

and, D^+ and $D^= = 0$, D^0 and D^- are given by

$$D^0 = 0.066e^{-3.44/kT} \quad \text{cm}^2/s \tag{1.70}$$

$$D^- = 12.0e^{-4.05/kT} \quad \text{cm}^2/s \tag{1.71}$$

Diffusivity of arsenic versus doping is plotted in figure 1.14.

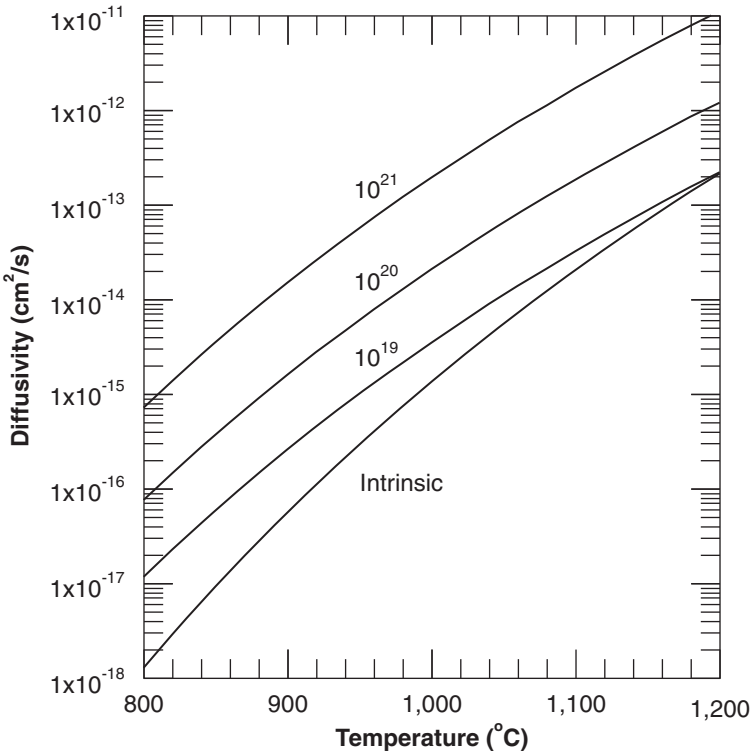

Figure 1.14: Diffusivity of arsenic in silicon versus temperature and arsenic concentration. Calculated form equations 7.68 through 7.71.

Arsenic has exactly the same tetrahedral diameter as silicon and so arsenic does not strain the silicon lattice or induce enhanced diffusivity in other dopants for T > ~700°C.

1.6.3. Diffusivity of boron in silicon

In Fair's model of diffusion, boron is assumed to diffuse exclusively by a vacancy mechanism under non-oxidizing conditions. Estimates of the interstitialcy component of boron diffusion are presented in table 1.2 and have recently been estimated at >98% [67].

In Fair's model boron diffuses by a B^+V^- vacancy pair with a migration energy approximately 0.5eV lower than other vacancy-ion pairs. Boron diffusivity is enhanced by p dopants when $p > n_i$ and reduced for $p < n_i$, boron diffusion is actually retarded in N type silicon where $n > n_i$.

The intrinsic diffusivity of boron is given by

$$D_i = 0.76e^{-3.46/kT} \quad \text{cm}^2/\text{s} \tag{1.72}$$

The extrinsic diffusivity of boron is given by

$$D_x = D^0 + D^+\left[\frac{p}{n_i}\right] \tag{1.73}$$

and D^- and $D^= = 0$, D^0 and D^+ are

$$D^0 = 0.037e^{-3.46/kT} \quad \text{cm}^2/\text{s} \tag{1.74}$$

and

$$D^+ = 0.76e^{-3.46/kT} \quad \text{cm}^2/\text{s} \tag{1.75}$$

The diffusivity of boron versus doping is plotted in figure 1.15

Boron is a faster diffuser than either phosphorus or arsenic. Boron has a tetrahedral radius of 0.82nms versus 1.18nms for silicon or a 0.75 mismatch ratio [3]. The relatively large size mismatch for boron versus silicon produces lattice strain that can lead to dislocation formation and reduced diffusivity. The strain introduced by boron into the silicon lattice can help to getter impurities by a trapping mechanism. High concentrations of boron are particularly good at gettering iron. Boron has a relatively low energy for interstitial formation of 2.26eV, therefore boron diffusivity is enhanced by oxidation. Figure 1.16 presents some data on oxidation enhanced boron diffusion.

The left side of figure 1.16 - 1.16a illustrates the increase in boron junction depth due to oxidation enhanced diffusion versus time for wet oxidation at 1,100°C. The right side of figure 1.16 - 1.16b illustrates the diffusivity of boron during dry oxygen oxidation versus an inert atmosphere versus temperature. Boron diffusion is enhanced during oxidation for both the intrinsic and extrinsic cases [15].

Boron forms stable oxides such as B_2O_5 and HBO_2 and readily segregates into the growing oxide during oxidation processes.

1.6.4. Diffusivity of phosphorus in silicon

The diffusivity of phosphorus is again explained as a vacancy dominated diffusion. Estimates of the interstitialcy component of phosphorus diffusion are presented in table 1.2. Phosphorus diffusion exhibits three distinct regions of behavior illustrated in figure 1.17

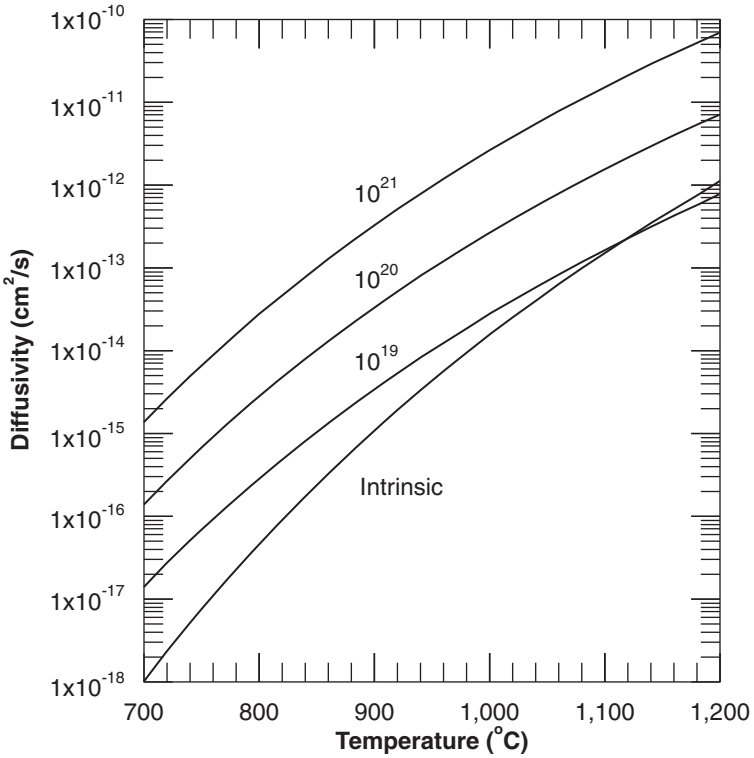

Figure 1.15: Diffusivity of boron in silicon versus temperature and boron concentration. Calculated from equations 1.72 through 1.75.

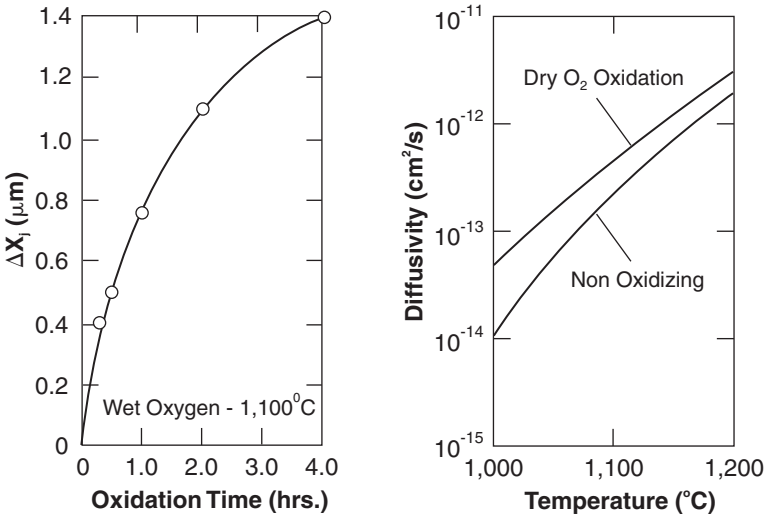

Figure 1.16: Oxidation enhancement of boron diffusivity [13],[14].

.

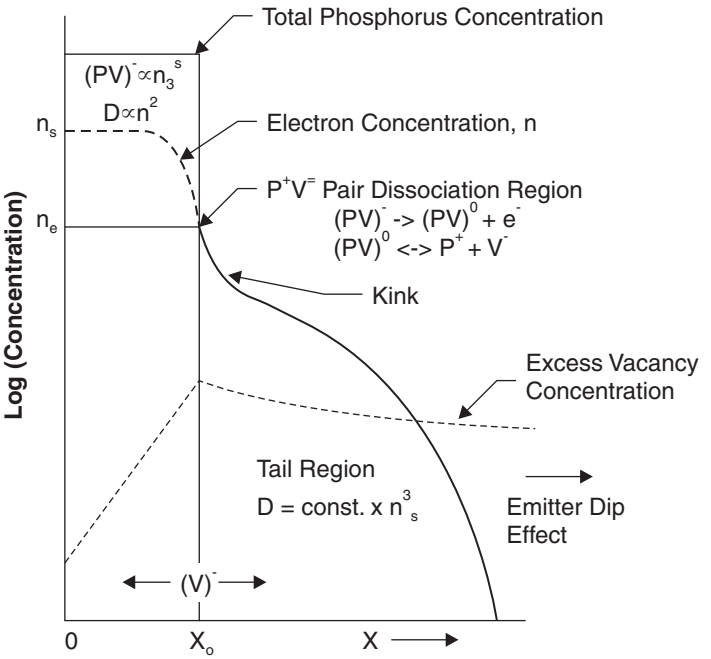

Figure 1.17: Phosphorus diffusion profile and vacancy model [6].

The phosphorus profile illustrated in figure 1.17 has three distinct regions:

1. The high concentration region where the total phosphorus concentration exceeds the free carrier concentration.
2. A kink in the profile
3. A tail region of enhanced diffusivity.

In the high concentration region a fraction of P^+ ions pair with $V^=$ vacancies as $P^+V^=$ pairs noted as $(PV)^-$. The concentration of $(PV)^-$ pairs is proportional to the surface electron concentration cubed (n_s^3), which has to be determined experimentally.

The intrinsic diffusivity of phosphorus is given by [6]

$$D_i = 3.85e^{-3.66/kT} \quad \text{cm}^2/\text{s} \tag{1.76}$$

In the high concentration region the extrinsic diffusivity of phosphorus is given by [6]

$$D_x = D^0 + D^= \left[\frac{n}{n_i}\right]^2 \tag{1.77}$$

and $D^- \sim 0$, $D^+ = 0$, D^0 and $D^=$ are given by

$$D^0 = 3.85e^{-3.66/kT} \quad \text{cm}^2/\text{s} \tag{1.78}$$

and

$$D^{=} = 44.2e^{-4.37/kT} \quad \text{cm}^2/\text{s} \tag{1.79}$$

Phosphorus has a tetrahedral radius of 0.110nms versus 0.118nms for silicon resulting in a mismatch ratio of 0.93 [3], and at high concentrations - phosphorus lattice strain can lead to defect formation. Fair and Tsai have proposed that tail formation in the phosphorus profile is due to dissociation of $P^+V^=$ pairs when n drops below 10^{20} /cm^3 at the diffusion front (the Fermi level is ~0.11eV from the conduction band), the $V^=$ vacancy changes state and the binding energy decreases enhancing the probability of disassociation and increasing the vacancy flux. Other researchers have found evidence of interstitialcy diffusion for phosphorus calling into question the physical correctness of the vacancy model [17],[18].

The electron concentration in the transition or "kink" region is given by

$$n_e = 4.65 \times 10^{21} e^{-0.39/kT} \quad \text{n/cm}^3 \tag{1.80}$$

The disassociation of the $(PV)^-$ pairs increase the vacancy concentration tail by

$$(PV)^- \rightarrow (PV)^X + e^- \tag{1.81}$$

and

$$(PV)^X \leftrightarrow P^+ + V^- \tag{1.82}$$

The diffusivity in the tail region increase as the V^- concentration increases and is given by [6]

$$D_{tail} = D^0 + D^- \frac{n_s^3}{n_e^2 n_i}[1 + e^{0.3/kT}] \quad \text{cm}^2/\text{s} \tag{1.83}$$

and

$$D^- = 4.44e^{-4/kT} \quad \text{cm}^2/\text{s} \tag{1.84}$$

Figure 1.18 illustrates the diffusivity of phosphorus versus temperature for the intrinsic and extrinsic cases. Figure 1.19 illustrates the diffusivity of phosphorus in the tail region.

The same $(PV)^-$ dissociation mechanism that creates enhanced diffusivity in the phosphorus "tail" can increase the diffusivity of dopants in junction pre-existing under phosphorus diffusions - see figure 1.20.

The effect of heavy phosphorus doping levels on co-diffusing species was first noted during emitter diffusion for bipolar transistors. The heavy phosphorus emitter was observed to increase the junction depth of the underlying boron doped base region relative to surrounding areas. The enhanced diffusion under the phosphorus emitters came to be known as "emitter push".

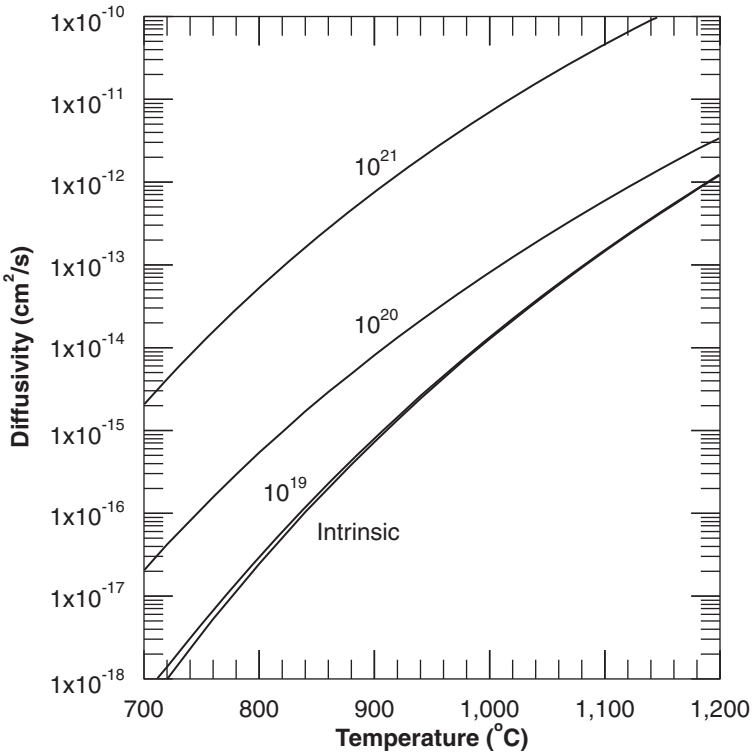

Figure 1.18: Phosphorus diffusivity in silicon versus phosphorus concentration and temperature - high concentration region. Calculated from equations 1.76 through 1.79.

Above 5 x 10^{20} phosphorus atoms/cm^3 the misfit lattice strain from the phosphorus introduces lattice strain (band gap narrowing) and reduces $(PV)^-$ pair dissociation. Figure 1.20 illustrates the increase in boron doped base junction depth versus phosphorus content for a 1,000C phosphorus emitter diffusion. The solid line is the increase in junction depth excluding the strain effect and the dotted line includes the strain effect, the round circles are experimental results.

The increase in base junction depth directly under the phosphorus diffusion is given by [21]

$$\delta(t) = W_0\left[\left(1+\frac{2D_{in}^{B}t}{W_0^2}\right)^{1/2} - \left(1+\frac{2Di^{B}t}{W_0}\right)^{1/2}\right] \tag{1.85}$$

where $\delta(t)$ is the increase in junction depth under the emitter diffusion and W_0 is a quantity related to the profile of the base diffusion prior to emitter diffusion.

W_0 is given by

$$W_0 = 0.4\frac{Q_0}{C_{p0}} \tag{1.86}$$

where, Q_0 is the integrated doping of the base, and C_{p0} is the peak concentration of the base dopant prior to emitter diffusion.
The diffusivity of boron under the emitter region is given by

$$D_{in}^{B} = D_i^{B}\frac{D_P^0 + D_P^-}{D_P^0} \tag{1.87}$$

where, $D_{in}{}^{B}$ is the diffusivity of the boron under the emitter, $D^0{}_P$ is the diffusivity of the phosphorus - neutral vacancy pair, and $D^-{}_P$ is the diffusivity of the phosphorus - negative vacancy pair.

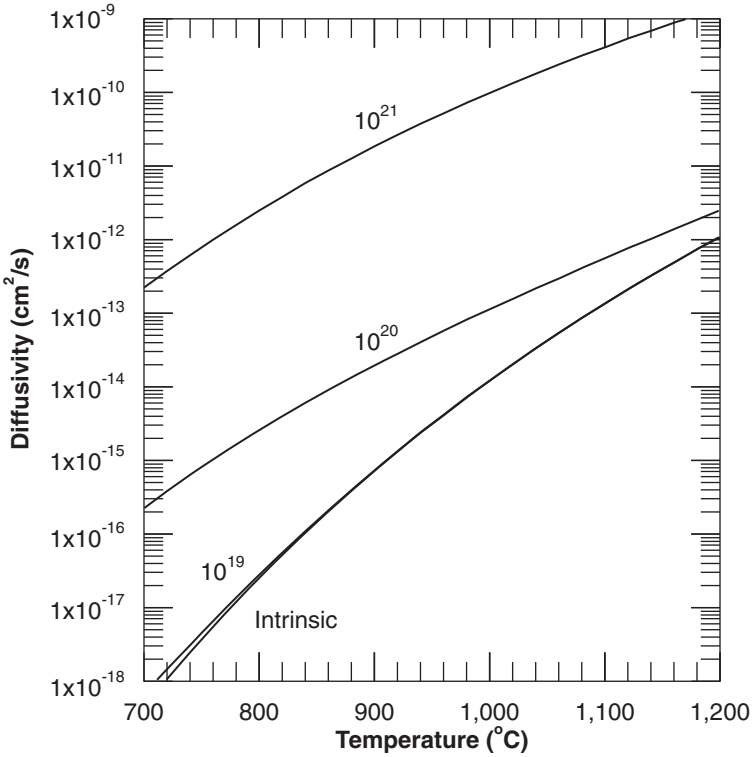

Figure 1.19: Phosphorus Diffusivity in silicon versus surface electron concentration and temperature - tail region. Calculated from equations 1.78, 1.83 and 1.84.

Phosphorus diffusivity (both intrinsic and extrinsic) is enhanced by oxidation (similar to boron) - see figure 1.22.

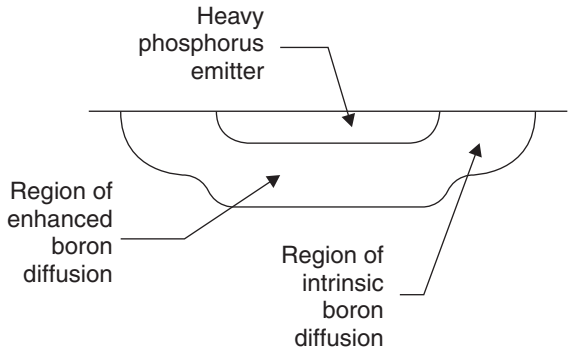

Figure 1.20: Enhanced diffusivity under heavy phosphorus doped regions - "emitter push".

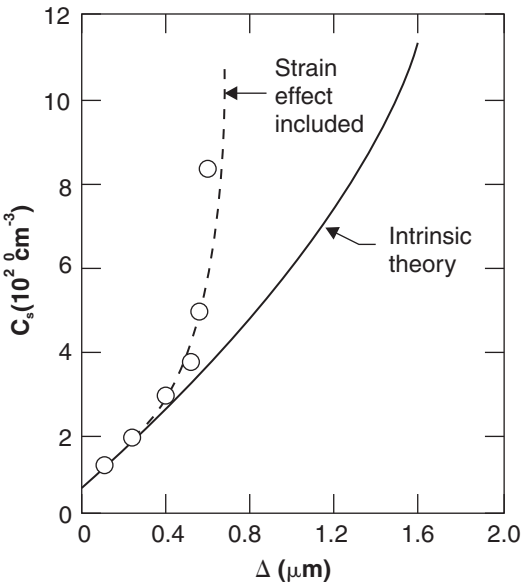

Figure 1.21: High concentration phosphorus induced strain effect on enhanced diffusion [21].

Figure 1.22 plots the ratio of diffusivity during oxidation to diffusivity under an inert ambient versus oxidation rate at four different temperatures. The data in figure 1.22 was generated by varying the oxygen partial-pressure and the initial oxide thickness to produce varying oxidation rates. For a given temperature the degree of diffusivity enhancement increases with increasing oxidation rate.

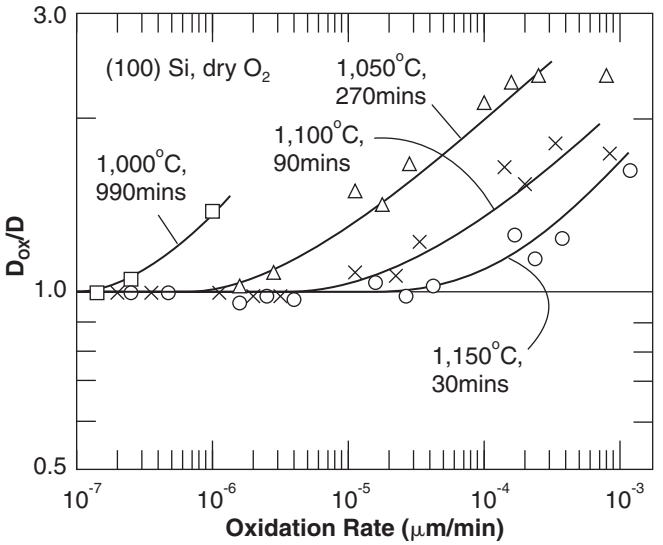

Figure 1.22: Phosphorus diffusivity enhancement versus oxidation rate. Adapted from [22]/

1.6.5. Diffusivity of miscellaneous dopants in silicon

In the preceding four sections the diffusivity of the four most common silicon dopants was discussed in detail. There are a a variety of other impurities whose diffusivity may be of interest. Table 1.4 presents a compilation of diffusivity values.

Table 1.4: Diffusivity of miscellaneous impurities in silicon.

Impurity	Temperature range (°C)	D_0 (cm^2/s)	E_a (eV)	Mechanism	Reference
Ag	1,100-1,300	$2x10^{-3}$	1.6	Interstitial	23
Al		0.5	3.0		28
		1,350	4.1		6
As (intrinsic)		22.9	4.1	Vacancy	6
Au	800-1,200	$1.1x10^{-3}$	1.12	Interstitial	23
Au (interstitial)	700-1,300	$2.4x10^{-4}$	0.39		23
Au (substitutional)	700-1,300	$2.8x10^{-3}$	2.04		23
B (intrinsic)		0.76	3.46	Vacancy	6
Bi		396	4.12		6
C		1.9	3.1		28
Co	900-1,200	$9.2x10^{-4}$	2.8		25

Table 1.4: Diffusivity of miscellaneous impurities in silicon.

Impurity	Temperature range (°C)	D_0 (cm^2/s)	E_a (eV)	Mechanism	Reference
Cr	1,100-1,250	0.01	1.0		24
Cu	800-1,100	$4.0x10^{-2}$	1.0	Interstitial	23
Cu (interstitial)		$4.7x10^{-3}$	0.43	Interstitial	23
Fe	1,100-1,250	$6.2x10^{-3}$	0.87	Interstitial	23
Ga		225	4.12		28
Ge		$6.26x10^{5}$	5.28		28
H_2		$9.4x10^{-3}$	0.48	Interstitial	23
He		0.11	1.26		28
In or Tl		16.5	3.9		28
		269	4.19		6
K	800-1,000	$1.1x10^{-3}$	0.76	Interstitial	23
Li	25-1,350	$2.3x10^{-3}$ to $9.4x10^{-4}$	0.63 to 0.78	Interstitial	23
N		0.05	3.65		6
Na	800-1,100	$1.6x10^{-3}$	0.76	Interstitial	23
Ni	450-800	0.1	1.9	Interstitial	23
O_2	700-1,240	$7x10^{-2}$	2.44		26
O (interstitial)	330-1,250	0.17	2.54	Interstitial	26
P (intrinsic)		3.85	3.66	Vacancy	6
Pt	800-1,100	$1.5x10^{2}$ to $1.7x10^{2}$	2.22 to 2.15	Interstitial	27
S		0.92	2.2	Interstitial	28
Sb (intrinsic)		0.214	3.65	Vacancy	6
Si (interstitial)		0.015	3.89	Vacancy	6
Sn		32	4.25		28
Zn		0.1	1.4	Interstitial	28

Figure 1.23 presents the values from table 1.4 in graphical form versus temperature, the graph is useful for comparing relative diffusivities.

As mentioned in previous sections, the size mismatch between a diffusing specie and the silicon lattice can result in lattice strain which may enhance the diffusivity of co-diffusing specie. Table 1.5 presents the relative sizes of selected impurities versus silicon.

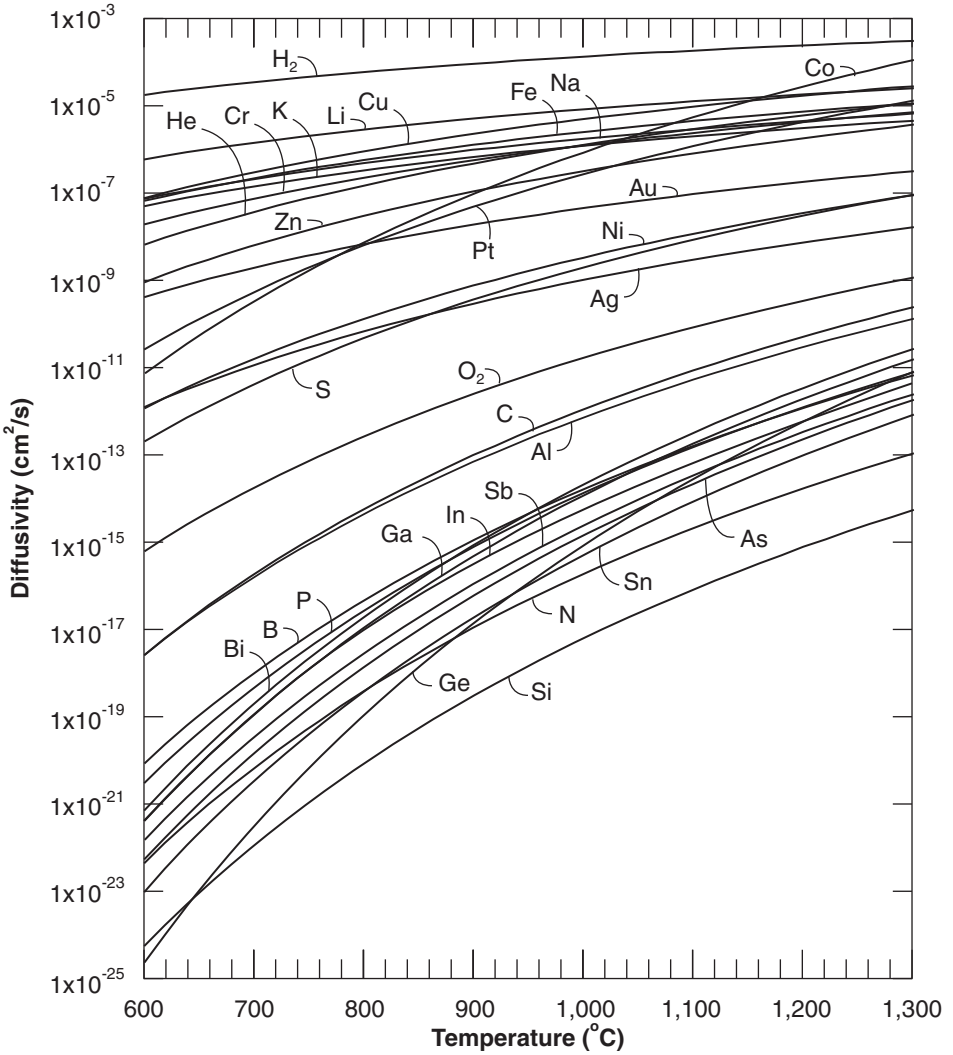

Figure 1.23: Diffusivities of selected impurities in silicon versus temperature - see table 1.4.

1.6.6. Diffusivity of impurities in polysilicon

Polysilicon is made up of grains of single crystal silicon randomly oriented relative to each other. Within the crystalline grains diffusion has characteristics similar to bulk single crystal silicon. In the grain boundaries diffusion can proceed at 100 times the rate of diffusion within the grains. Because the grain boundaries dominate polysilicon diffusion, grain size and hence the grain boundaries determine the diffusivity of impurities in the polysilicon film.

Table 1.5: Size of impurity atoms relative to silicon [3].

Element	Tetrahedral radius (nm)	Size relative to silicon
Aluminum	0.126	1.07
Gallium	0.126	1.07
Gold	0.150	1.27
Indium	0.144	1.22
Silicon	0.118	1.00

The grain size for polysilicon can range from 0.1 to 20μms in size and depends on the polysilicon deposition conditions and thickness, the underlying film, and the subsequent thermal history of the film. Due to the number of variables that effect grain size and the dominant role of grain boundaries in polysilicon diffusion, diffusivities reported by various researchers vary widely and it is difficult to make definitive predictions. Table 1.6 presents some reported values for impurity diffusion in polysilicon.

Table 1.6: Diffusivity for miscellaneous impurities in polysilicon [41].

Impurity	Temperature range (^oC)	D_0 (cm^2/s)	E_a (eV)	Mechanism	System	Reference
As	700-1,050	0.28	2.8	-----	RTP	30
	800-1,000	$8.4x10^4$	3.8	Tail region	RTP	31
	800-1,000	1,700	3.8	Peak region	RTP	31
	750-950	$8.6x10^4$	3.9	Grain-bound	Furnace	37
	700-850	10	3.36	Grain-bound	Furnace	38
	950-1,100	0.63	3.22	Combined	Furnace	39
	700-1,000	1.66	3.22	Combined	Furnace	36
B	1,000-1,200	$6.6x10^{-4}$	1.87	Grain-bound	Furnace	32
P	800-1,000	$1.9x10^{-2}$	1.76	Grain-bound	RTP	29
	1,100-1,200	$4.0x10^{-3}$	1.71	Grain-bound	Furnace	33,32
	900-1,100	$5.3x10^{-5}$	1.95	Grain-bound	Furnace	34
	700-850	44.8	3.4	Combined	Furnace	35
	700-1,100	1.0	2.75	Combined	Furnace	36
	700-1,050	1.81	3.14	-----	Furnace	30
Sb	1,050-1,150	13.6	3.9	Bulk	Furnace	40
	1,050-1,150	812	2.9	Grain-bound	Furnace	40

Figure 1.24 illustrate the diffusivity of selected impurity in polysilicon versus temperature from table 1.4 in graphical form to allow easy comparisons of relative diffusivities.

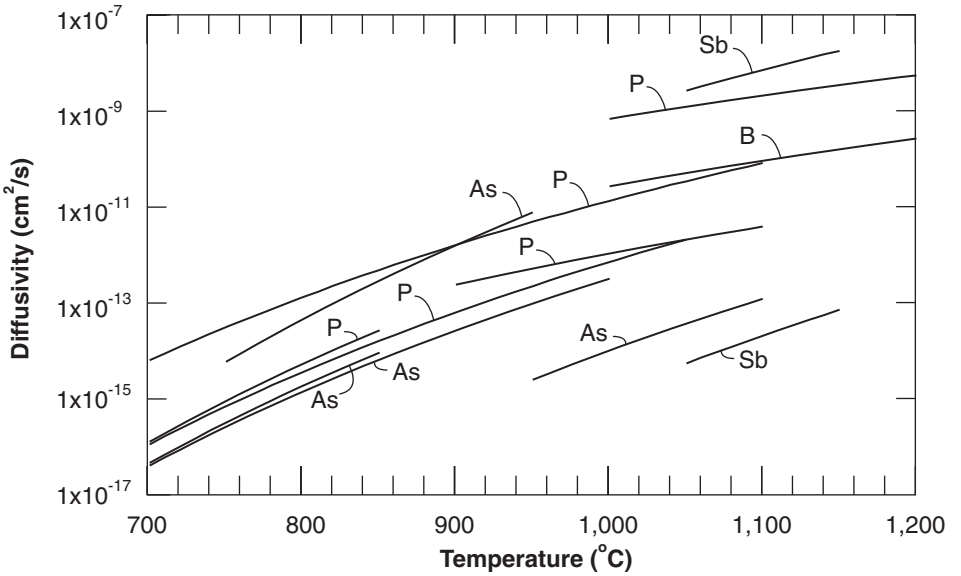

Figure 1.24: Diffusivities of selected impurities in polysilicon - see table 7.4.

1.6.7. Diffusivity of impurities in silicon dioxide

Silicon dioxide is often used to mask against impurity diffusion during pre-deposition - see figure 1.8. Silicon dioxide may also become inadvertently doped by ion implantation during processing. It is therefore important to be able to calculate the diffusion of impurities through silicon dioxide. Table 1.7 presents the diffusivity of selected impurities in silicon dioxide.

Table 1.7: Diffusivity of selected impurities in silicon dioxide.

Impurity	D_0 (cm^2/s)	E_a (eV)	Source and ambient	Reference
As	67.25	4.7	Ion implant, N_2	43
	$3.7x10^{-2}$	3.7	Ion implant, O_2	43
Au	$8.2x10^{-10}$	0.8		44
	$1.52x10^{-7}$	2.1		44
B	$7.23x10^{-6}$	2.38	B_2O_3 vapor, N_2+O_2	42
	$1.23x10^{-4}$	3.39	B_2O_3 vapor, Ar	42
	$3.16x10^{-4}$	3.53	Borosilicate	42
D_2	$5.01x10^{-4}$	0.455		46
Ga	$1.04x10^{5}$	4.17	Ga_2O_3 vapor, H_2+N_2+H_2O	42
H^+	1	0.73		46
H_2	$5.65x10^{-4}$	0.446		44

Table 1.7: Diffusivity of selected impurities in silicon dioxide.

Impurity	D_0 (cm^2/s)	E_a (eV)	Source and ambient	Reference
He	$3x10^{-4}$	0.24		44
H_2O	10^{-6}	0.79		44
O_2	$2.7x10^{-4}$	1.16		44
OH	$9.5x10^{-4}$	0.68		46
Na	6.9	1.3		44
P	$5.73x10^{-5}$ $1.86x10^{-1}$	2.20 4.03	P_2O_5 vapor, N_2 Phosphosilicate glass, N_2	42 45
Pt	$1.2x10^{-13}$	0.75		44
Sb	$1.31x10^{16}$	8.75	Sb_2O_5 vapor, O_2+N_2	42

Figure 1.25 presents the diffusivity values from table 1.6 in graph form for easier comparison. The diffusivities presented in table 1.6 for arsenic, boron and phosphorus are nitrogen ambient diffusion values. Boron and phosphorus are vapor sources and arsenic is an ion implanted source.

1.6.7.1. Diffusivity of boron in silicon dioxide

As IC minimum feature sizes have shrunk the diffusion of boron through silicon dioxide has taken on an increasingly critical aspect. When MOSFET minimum features were above approximately 0.5μms, the gate polysilicon was doped N-type with phosphorus. As minimum features have shrunk below approximately 0.5μms, adequate PMOS performance cannot be achieved without doping the PMOS gate polysilicon P-type. For <0.5μm minimum feature size devices, the NMOS polysilicon is phosphorus doped and the PMOS polysilicon is boron doped. Boron is readily taken up by oxide (see section 1.81), and boron can diffuse through the thin gate oxide layer and dope the channel resulting in uncontrolled shifts in the PMOS device threshold voltage. The diffusion of boron through silicon dioxide may be increased through interactions with other species.

One technique for introducing boron into device structures is ion implantation of BF_2 ions. Fluorine from the BF_2 ions increases the diffusivity of boron in silicon dioxide. The diffusivity of boron in the presence of fluorine is given by [66]

$$D(BF_2) = 1.1x10^{-3}(0.33 + 1.1x10^{-6}\phi F_2^{1/2})e^{-3.56/kT} \tag{1.88}$$

where, ϕF_2 is the BF_2 dose in atoms/cm^2.

Hydrogen also increases the diffusivity of boron in silicon dioxide given by [66]

$$D(H_2) = 3.63x10^{-4}e^{-3.56/kT} + [H_2]^{1/2} \cdot 2.65x10^{-5}e^{-3.0/kT} \tag{1.89}$$

where, H_2 is the percent of H_2 in the diffusing ambient.

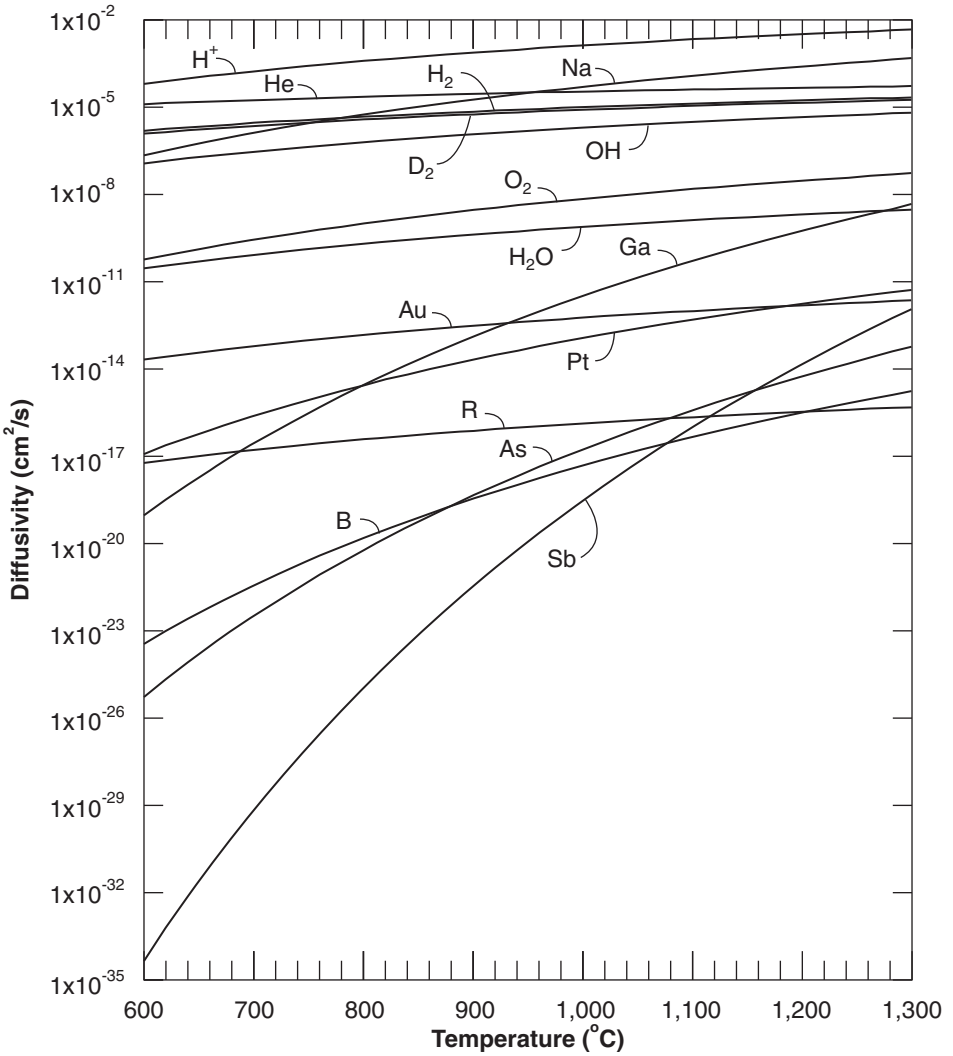

Figure 1.25: Diffusivity of selected impurities in silicon dioxide versus temperature - data from table 1.7.

Equation 1.88 for fluorine effects and equation 1.89 for H_2 effects on boron diffusion in silicon dioxide are presented in the left and right side of figure 1.26 respectively.

Boron diffusivity in silicon dioxide is also believed to be increased by SiO content and therefore by decreasing silicon dioxide thickness [66].

1.7. Solid solubility

Steady state solid solubility is defined as:

- The maximum concentration of a substance that can be dissolved in a solid at a given temperature.

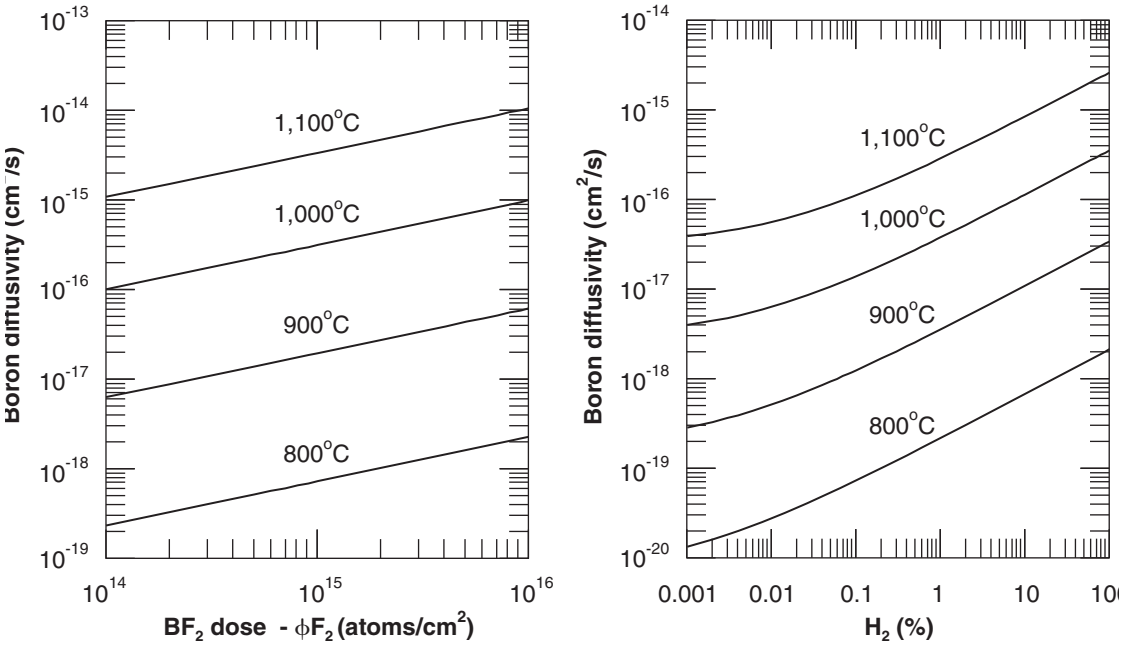

Figure 1.26: Effect of fluorine and hydrogen on boron diffusivity in silicon dioxide [66].

The first attempt to summarize experimental data for the solid solubility of impurities in silicon was performed by Trumbore in 1960 [47]. Recently Borisenko and Yudin reexamined the solid solubility curves for antimony, arsenic, boron and phosphorus utilizing newer more accurate data [48] - see figure 1.27.

The data presented in figure 1.27 represents the solid solubility, not the electrically active dopant. Dopants introduced into silicon may occupy interstitial or substitutional positions in the silicon lattice, or form clusters, i.e. arsenic - see the next section. The method of introducing a dopant into silicon and subsequent heat treatments determine the amount of dopant that contributes free carriers, i.e., is electrically active. Prior to annealing a significant percentage of a dopant may be electrically inactive.

1.7.1. Solid solubility of arsenic in silicon

Arsenic forms clusters when concentrations in silicon are in excess of 10^{20} atoms/cm^3. It is believed that 3 arsenic atoms and one electron form a cluster that is electrically active at high temperature and is neutral at room temperature [49].

The model for clustering is

$$3As^{+} + e^{-} \overset{\text{high temp}}{\leftrightarrow} As_3^{2+} \overset{\text{room temp}}{\leftrightarrow} As_3 \tag{1.90}$$

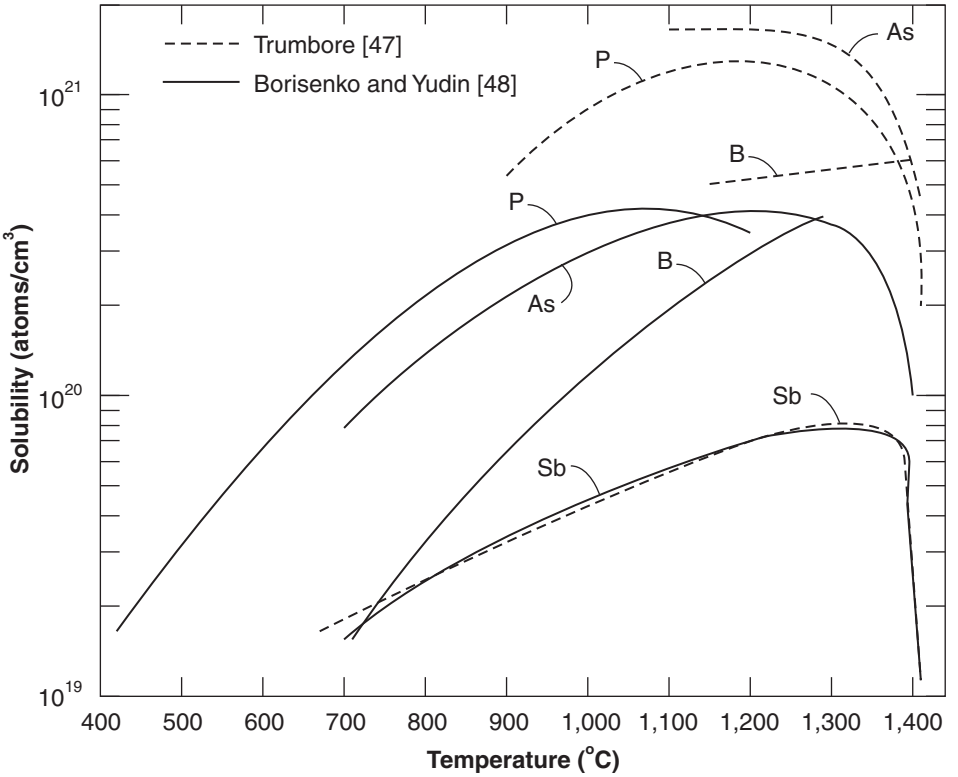

Figure 1.27: Solid solubility of common dopants in silicon. Summarized from [47],[48].

A generalized model of arsenic clustering has been derived [50], and the expression for C_{max} versus temperature is given by

$$C_{max} = 1.896x10^{22}e^{-0.453/kT} \quad \text{atoms/cm}^3 \tag{1.91}$$

1.7.2. Solid solubility of boron in silicon

There is no physical model for electrically active boron concentrations - the values have to be found experimentally.

1.7.3. Solid solubility of phosphorus in silicon

At high concentration the expression for the total electrically active phosphorus concentration is given by [44]

$$C_T = n + 2.4x10^{-43}n^3 \quad \text{atoms/cm}^3 \tag{1.92}$$

where, n is the electron concentrations or electrically active phosphorus concentration. Equation 1.92 is valid from 900 to 1,050°C.

For arsenic, boron, and phosphorus in silicon the maximum electrically active dopants match up well with the solid solubility curves of Borisenko and Yudin presented in figure 1.25.

1.7.4. Solid solubility of miscellaneous dopants in silicon.

Figure 1.28 present additional solid solubility data covering impurities not included in figure 1.27. The data in figure 1.28 comes from Trumbore [47], updated curves for these impurities are not available.

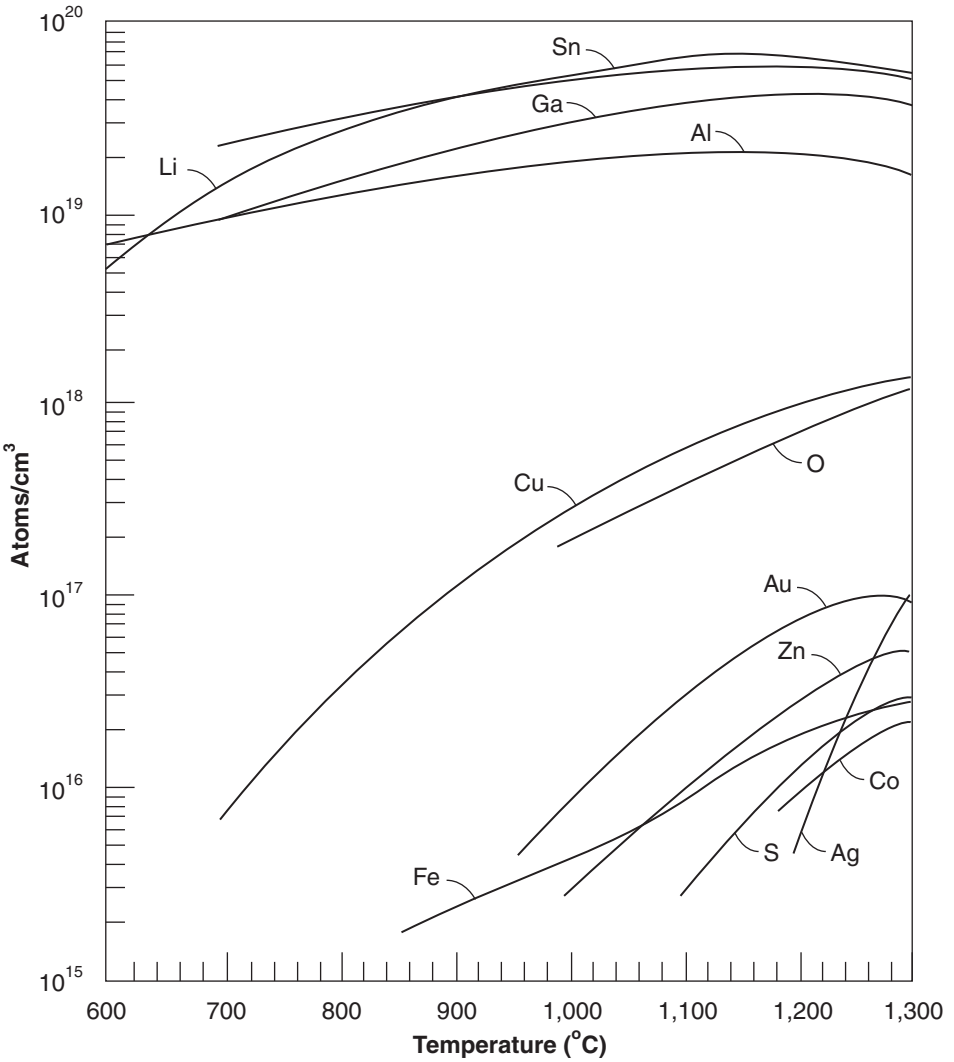

Figure 1.28: Solid solubility of selected impurities in silicon [47].

1.8. Deviations from simple diffusion theory

In the preceding sections the basics of diffusion theory have been presented, in this section the complications of selected real world diffusion problems will be examined.

1.8.1. Redistribution of impurities during thermal oxidation

In section 1.5.2 the solution for two step or drive-in diffusions was presented. One of the assumptions was constant Q during diffusion. It is very unusual for a drive-in diffusion to be performed without simultaneous oxidation during at least some part of the cycle. It has been found that impurities are redistributed in silicon near a growing thermal oxide [55]. Redistribution is due to several factors. If any two phases - solid, liquid or gas are brought into contact an impurity found in either of the two phase will redistribute between the two phase until equilibrium is reached. In equilibrium the ratio of the concentrations of the impurity in the two phases will be constant.

- Segregation Coefficient - the ratio of the concentration of an impurity in one phase to the concentration of the impurity in a second under equilibrium.

  The segregation coefficient m, for the Si - SiO_2 system is defined as

$$m = \frac{\text{Equalibrium concentration of impurity in silicon}}{\text{Equalibrium concentration of impurity in silicon dixoide}} \tag{1.93}$$

Another factor effecting impurity redistribution during oxidation is the diffusivity of the impurity in silicon dioxide. If the impurity has a high diffusivity in silicon dioxide the impurity can “escape” through the oxide layer. If the impurity has a low diffusivity in silicon dioxide then the impurity will be trapped in the silicon. Figure 1.29 illustrates four possible impurity profiles due to oxidation.

The third factor in redistribution is the moving oxide-silicon interface. Even if an impurity has a segregation coefficient of 1, the increase in volume occupied by oxide over silicon will result in a decrease in the impurity concentration in the oxide layer.

Figure 1.29 illustrates four cases of impurity segregation. 1.29a and b illustrate the cases where oxide takes up the impurity with low diffusivity in the oxide 1.29a, and fast diffusivity in the oxide 1.29b. 1.29c and d illustrate the cases where the oxide rejects the impurity with low diffusivity in the oxide 1.29c and fast diffusivity in the oxide 1.29d.

A theory on the redistribution process has been proposed [56]. The assumptions are:

1. The concentration of the impurity at the oxide-gas boundary is constant.
2. Deep inside the silicon the impurity concentration approaches the background concentration of the silicon.
3. The segregation coefficient ratio is maintained.
4. The impurity is preserved at the oxide-silicon interface.
5. The oxidation rate is parabolic and given by:

$$x_o = \sqrt{Bt} \tag{1.94}$$

The resulting expression for the concentration on the silicon side of the interface is

$$\frac{C_S}{C_B} = \frac{1 + (C_O/C_B)\lambda}{1 + (1/m - \alpha)\sqrt{\pi}\exp(\alpha^2 B/4D)erfc(\alpha\sqrt{B/4D})\sqrt{B/4D} + \lambda/m} \tag{1.95}$$

and

$$\lambda \equiv \frac{r\exp[(\alpha^2 r^2 - 1)B/4Dr^2]erfc(\alpha\sqrt{B/4D})}{erf(\sqrt{B/4D_O})} \tag{1.96}$$

and

$$r \equiv \sqrt{D_O/D} \tag{1.97}$$

where, D is the diffusivity in silicon, D_O is the diffusivity in oxide, α is the ratio of the thickness of silicon consumed during oxidation to the thickness of oxide produced (0.45). One interesting feature of the theory is that the interface will reach a steady state concentration irrespective of oxidation time.

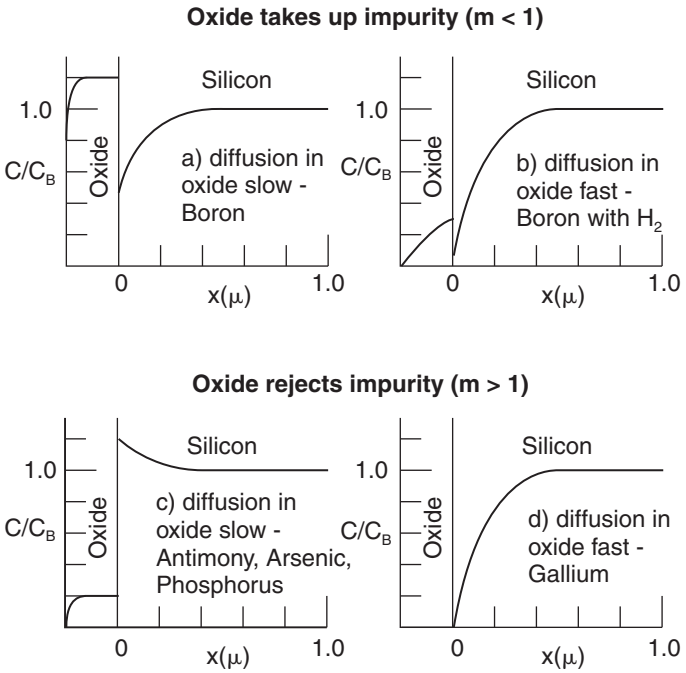

Figure 1.29: Impurity redistribution in silicon due to thermal oxidation [5].

Table 1.7 presents some values for segregation coefficient.

Based on equations 1.95 through 1.97 and the values in table 1.7 the ratio of the surface concentration of impurity to the background concentration can be calculated.

Table 1.8: Segregation coefficient of impurities at the silicon-silicon dioxide interface.

Impurity	Segregation coefficient	Reference
As	~10	56
	~800	58
	~1,000-,2000	59
B	~0.3	56
	0.03exp(0.52/kT) for (100)	57
	0.05exp(0.52/kT) for (111)	58
	~0.1-0.3	59
P	~10	56
	~2,000-3,000	59
Sb	~10	56

Figures 1.30 through 1.32 illustrate the segregation phenomena for arsenic, boron and phosphorus under oxygen and steam oxidation conditions. In each case steam creates a greater segregation phenomena due to the greater oxidation rate of steam over oxygen. Figure 1.30 through 1.32 are calculated from equation 1.95 using Grove's values for segregation for arsenic and phosphorus [56] and Kolby and Katz value for boron (100) [57].

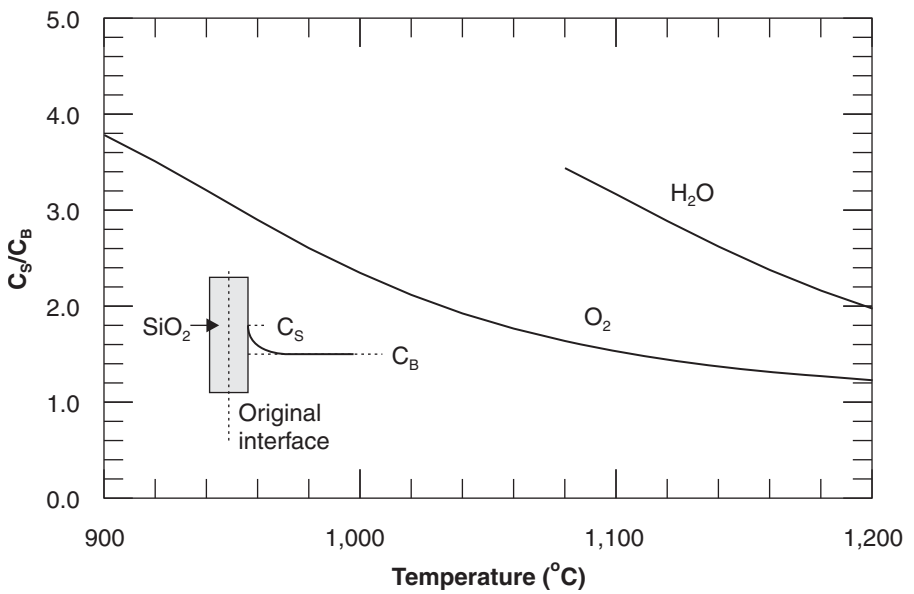

Figure 1.30: Surface concentration versus temperature for arsenic following oxidation.

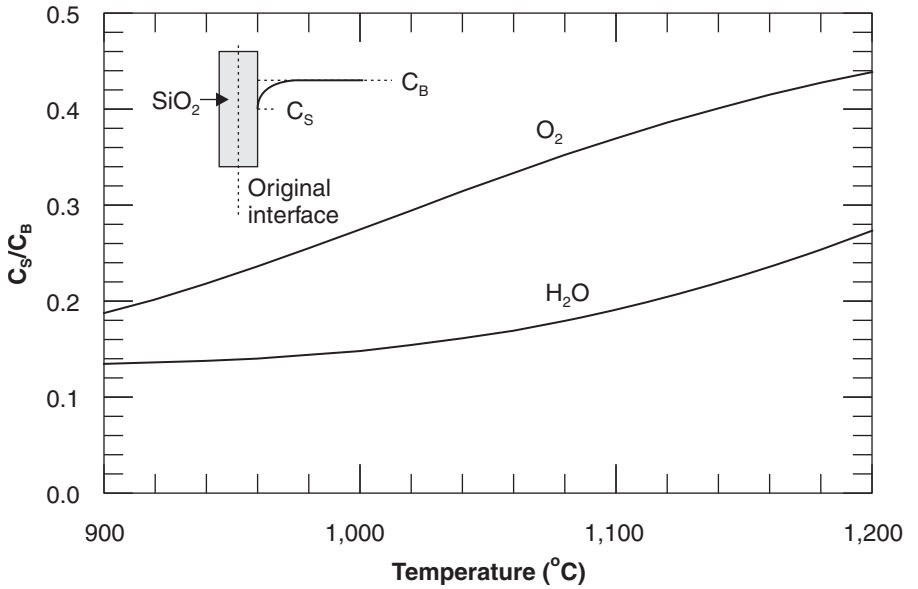

Figure 1.31: Surface concentration versus temperature for boron following oxidation.

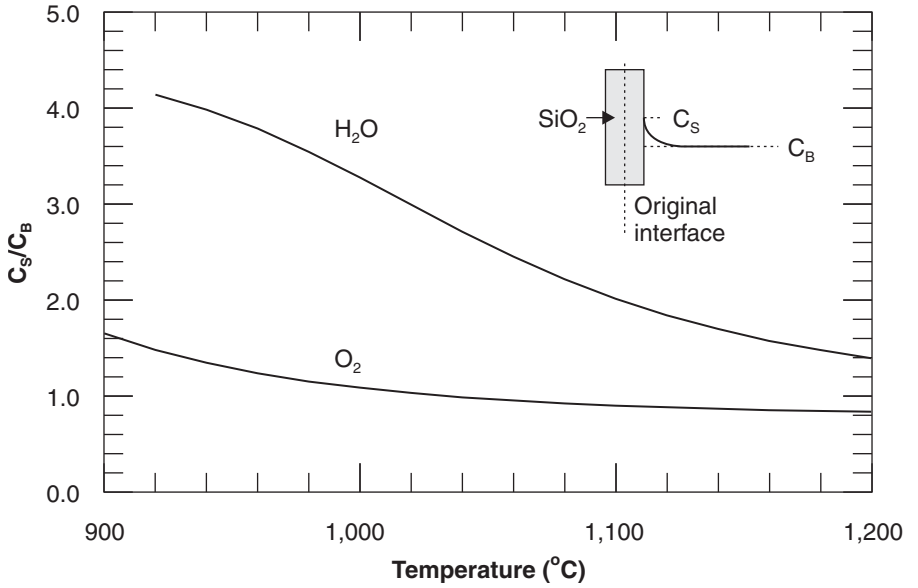

Figure 1.32: Surface concentration versus temperature for phosphorus following oxidation.

The distance over which the segregation effect influences the impurity profile is the diffusion length given by 2 times the square root of Dt. Figure 1.33 illustrates boron segregation versus oxidation temperature [60].

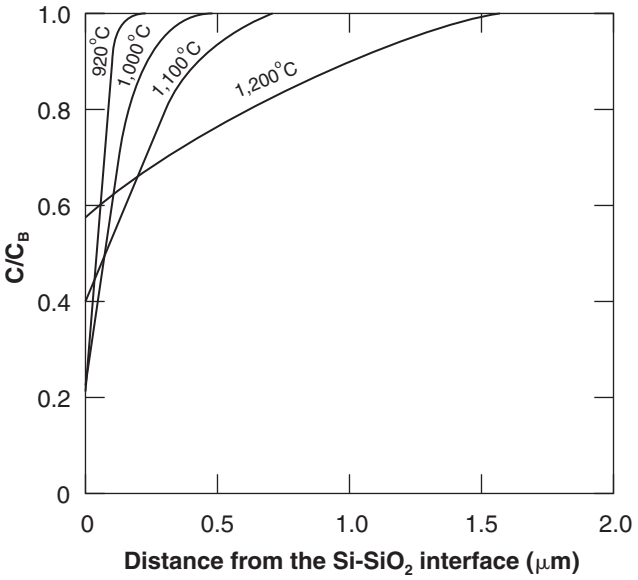

Figure 1.33: Calculated boron concentration versus distance after dry oxygen oxidation to produce a 0.2μm thick oxide at various temperatures [60].

1.8.2. Diffusion through an oxide mask

The diffusion discussions presented in preceding sections are all based on one-dimensional diffusion. During pre-deposition - the deposition process is made selective by utilizing an oxide layer to block pre-deposition in unwanted areas and to diffuse the dopant into the silicon through windows in the oxide where the dopant is desired (see figure 1.34).

During pre-deposition the dopant enters the silicon where the oxide is missing and is blocked by the oxide where the oxide is present. The dopant diffusing into the silicon vertically, also laterally diffuses under the oxide window. Solving the diffusion equations for the two dimensional problem reveals that dopant diffuses more slowly parallel to the surface than normal to the surface (the parallel diffusion is 75 to 85% of the normal diffusion). Figure 1.35 illustrates equal concentrations contours for a pre-deposition (complementary error function) diffusion - figure 1.35a and a drive-in (gaussian) diffusion - figure 1.35b.

1.8.3. Oxide thickness to mask against diffusion

If a silicon dioxide layer is utilized to create a selective doping process it is necessary to determine the thickness of oxide required to block the pre-deposition process. In order to calculate the oxide thickness required to block deposition, consider pre-deposition through an oxide layer schematically illustrated in figure 1.36.

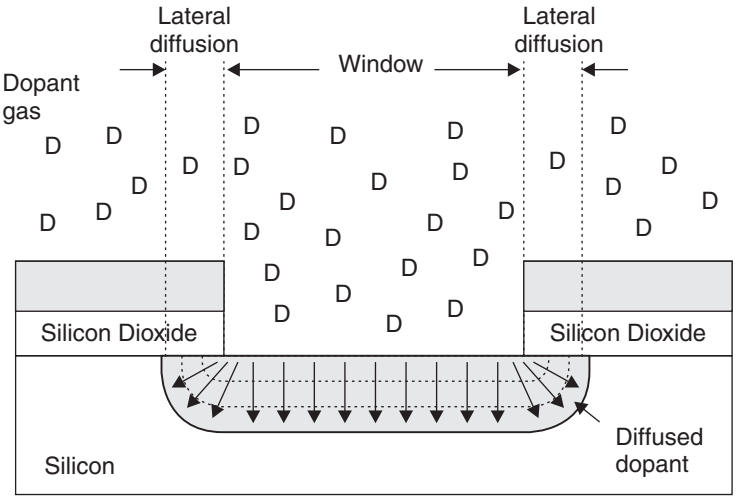

Figure 1.34: Pre-deposition through a silicon dioxide window.

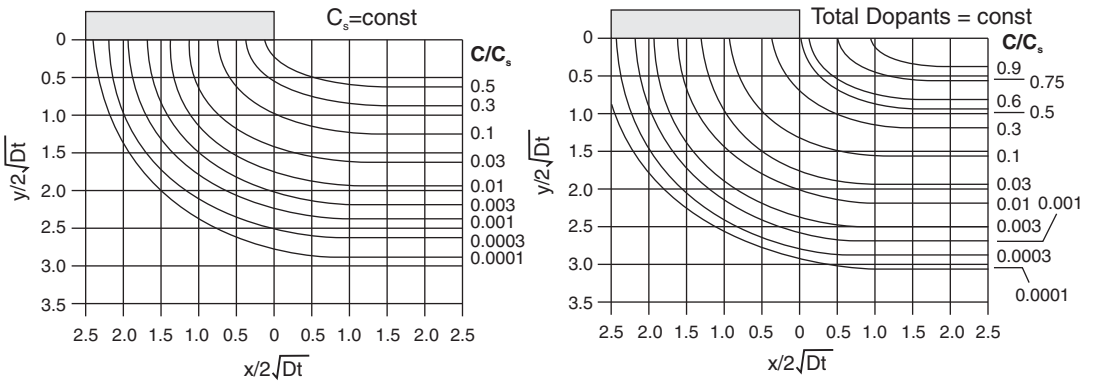

a) Complementary error function **b) Gaussian**

Figure 1.35: Lateral diffusion profiles [52].

The assumptions used to solve the problem are:

1. The concentration at the surface of the oxide layer C_o and the oxide thickness x_o are both constant throughout the pre-deposition process.
2. The concentration goes to zero deep inside the silicon.
3. The ratio of the concentrations on either side of the oxide-silicon interface are determined by the segregation coefficient m.
4. The flux of impurities through the interface is continuos.

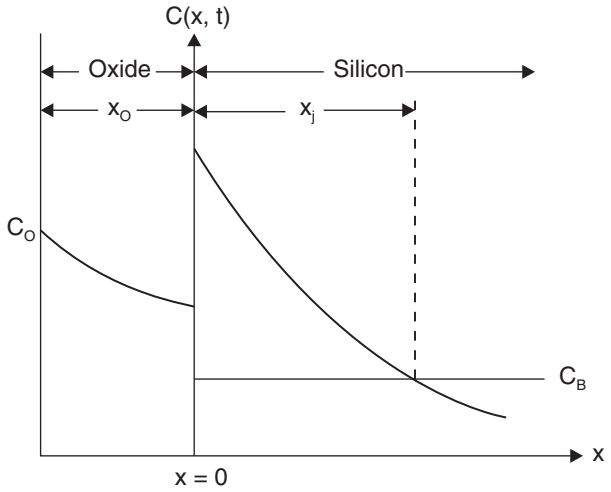

Figure 1.36: Impurity distribution from pre-deposition through an oxide [5].

The solution to this problem is given by an infinite series [53]. For small values of x such that

$$x \ll \sqrt{D/D_O x_O} \tag{1.98}$$

then the solution may be approximated by the first term in the series [5]

$$\frac{C(x,t)}{C_O} = \frac{2mr}{m+r} erfc\left[\frac{x_O}{2\sqrt{D_O t}} + \frac{x}{2\sqrt{Dt}}\right] \tag{1.99}$$

The solution for the junction depth x_j is given by the conditions which when substituted into equation 1.99 result in

$$\frac{x_j}{\sqrt{t}} = -\frac{1}{r}\frac{x_O}{\sqrt{t}} + I \tag{1.100}$$

and

$$I \equiv 2\sqrt{D}\arg\left[\frac{(m+r)C_B}{2mrC_O}\right] \tag{1.101}$$

The oxide thickness required to mask against pre-deposition can now be found by setting $x_j = 0$ in equation 1.100 Figure 1.36 presents empirical data on oxide thickness to mask against pre-deposition [54].

1.8.4. Diffusion from a uniformly doped oxide layer

A doped oxide layer can be deposited on silicon and used as a doping source. Figure 1.38 presents a schematic representation of diffusion from a doped oxide layer.

For relatively short diffusion time such that

$$x_O > 4\sqrt{D_O t} \tag{1.102}$$

then

$$C(x,t) \cong \frac{C_O\sqrt{D_O/D}}{(1+k)} erfc\left(\frac{x}{2\sqrt{Dt}}\right) \tag{1.103}$$

and

$$k = \frac{1}{m}\sqrt{D_O/D} \tag{1.104}$$

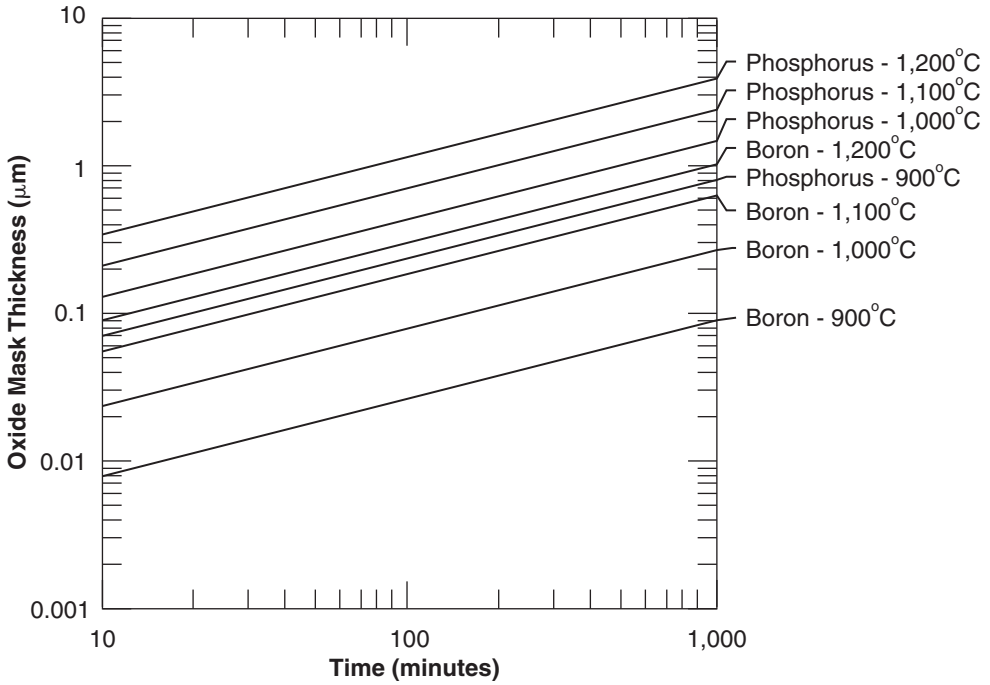

Figure 1.37: Oxide thickness to mask against deposition [54].

For longer diffusion times or thin oxide [61]

$$C(0,t) \approx \frac{C_O rm}{m+r}[1 - 2erfc(\phi_O) + 2erfc(2\phi_O)] \tag{1.105}$$

and

$$C(x,t) \approx \frac{C_O rm}{m+r}[erfc(\phi) - 2erfc(\phi_O + \phi) + erfc(2\phi_O\phi)] \tag{1.106}$$

where

$$\phi_O = \frac{x_O}{2\sqrt{D_O t}} \tag{1.107}$$

and

$$\phi = \frac{x}{2\sqrt{Dt}} \tag{1.108}$$

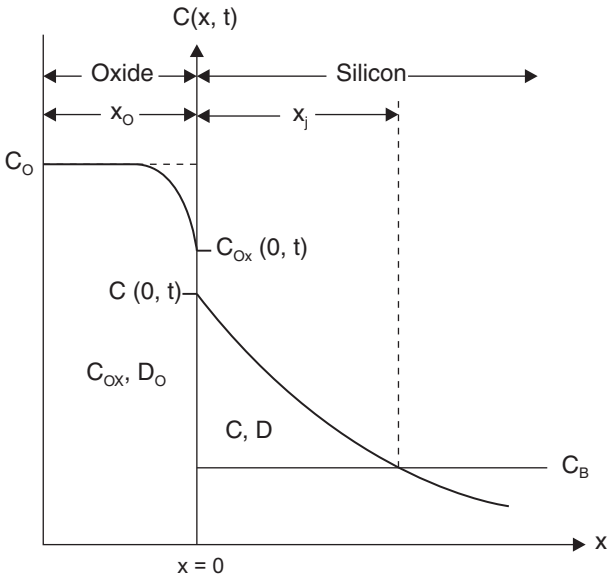

Figure 1.38: Schematic of diffusion from a uniformly doped oxide layer [61].

1.8.5. Solving for junction depth

It is often useful to define a diffused impurity profile by the junction depth. The junction depth for pre-deposition is given by

$$x_j = 2\sqrt{Dt}\ erfc^{-1}(C_S/C_B) \tag{1.109}$$

and for drive-in by

$$x_j = [4Dt\ln(Q/C_S\sqrt{\pi Dt})]^{1/2} \tag{1.110}$$

1.8.6. Successive diffusions

During integrated circuit fabrication multiple high temperature processes are used in succession. Each subsequent thermal process further diffuses any impurities present in the silicon substrate. The effect of successive diffusions is calculated by summing the Dt as follows

$$Dt_{tot} = \sum D_1 t_1 + D_2 t_2 + D_3 t_3 + \ldots \tag{1.111}$$

1.8.7. Ramping

In order to prevent crystallographic damage and wafer warpage due to thermal gradients, wafers are most commonly inserted into diffusion furnaces at a relatively low temperature and then the furnace temperature is increased to the process temperature at a controlled rate - referred to as ramping the furnace. At the completion of processing the furnace temperature is once again ramped down to a lower temperature for the wafers to be removed from the furnace. Most commonly a temperature of 750^{o}C is used for inserting and removing wafers from a diffusion furnace. 750^{o}C provides manageable thermal stresses, is a temperature from which a furnace can reach a process temperature and return in a reasonable amount of time, and is above the transition temperature for devitrification of the quartware commonly used in furncaes. The ramp rate employed in different types of thermal processors are presented in table 1.7.

Table 1.9: Thermal processor ramp rates

Processor	Ramp up rate	Ramp down rate
Conventional batch furnace	5-10^{o}C/min.	2-3^{o}C/min.
Rapid ramp batch furnace	80-100^{o}C/min.	60^{o}C/min.
Single wafer rapid thermal processor	25-100^{o}C/sec.	30-50^{o}C/sec.

For a conventional furnace the time to ramp from 750^{o}C to a process temperature hundreds of degrees higher can result in significant Dt during ramping, the Dt resulting from furnace ramping may be calculated as follows [2] (note here that the much faster ramp rates of rapid ramp furnaces and rapid thermal processor systems allow Dt during ramping to be minimized, the importance of low Dt ramping will be discussed in chapter 8)

Assume a furnace is being ramped down at a linear rate C such that

$$T(t) = T_{proc} - Ct \tag{1.112}$$

where, T_{proc} is the processing temperature from which the ramp occurs.

The effective Dt is therefore

$$(Dt)_{eff} = \int_0^{t_0} D(t)dt \tag{1.113}$$

where the ramp down occurs for a time t_0. Given that ramping is typically carried out until the diffusivity is negligibly small, the integral can be approximated by taking the upper limit as infinity, since

$$\frac{1}{T} = \frac{1}{T_{proc} - Ct} \cong \frac{1}{T_{proc}}\left(1 + \frac{Ct}{T_{proc}} + \ldots\right) \tag{1.114}$$

and substituting equation 7.114 into the arhenius equation for diffusivity, equation 1.63, gives

$$D(t) = D_0 \exp\left[-\frac{E_a}{kT_{proc}}\left(1 + \frac{Ct}{T_{proc}} + \ldots\right)\right] = D(T_{proc})e^{-(CE_a/kT_{proc}^2)t} \tag{1.115}$$

where, $D(T_{proc})$ is the diffusivity at T_{proc}. Substituting into equation 1.113 and using infinity as the upper integration limit gives

$$(Dt)_{eff} \cong D(T_{proc})\left[\frac{kT_{proc}^2}{CE_a}\right] \tag{1.116}$$

1.8.8. Deposition from a gas phase

Current state-of-the-art integrated circuit fabrication utilizes ion implantation to introduce impurities into silicon, however trailing edge processes may still utilize gas phase deposition to dope polysilicon. Legacy processes still in use may also utilize gas phase deposition processes for general doping.

Henry's law relates the partial pressure of the impurity in the gas phase p to the surface concentration, as

$$C_S = Hp \tag{1.117}$$

where H is Henry's gas law constant.

The surface concentration therefore depends on the partial pressure of the dopant in the gas (until the surface reaches solid solubility). Same of the candidate doping sources for gas phase deposition are listed in table 1.9.

The gaseous sources listed in table 1.9, arsine, diborane and phosphine are generally avoided for open furnace use due to their high toxicity (these gases are used in closed deposition systems for in-situ doping - see chapter 10). the most commonly used sources are spin-on arsenic for buried layers, boron tribromide and phosphorus oxychloride for junction formation. Boron and phosphorus solid source discs are also widely used.

Boron tribromide and phosphorus oxychloride are both liquids at room temperature. In order to introduce these sources into a diffusion furnace as a gaseous source an inert gas such as nitrogen is bubbled through the liquids at a controlled flow rate and temperature. The mole fraction of dopant entering the gas is given by

$$M = \frac{p_l V_C}{p_C \times 22,400} \tag{1.118}$$

where, M is the molar flow rate in moles/min., p_l is the vapor pressure of the liquid at the bubbler temperature in mm of Hg, p_C is the pressure of the carrier gas in mm of Hg (mm of Hg equals PSI multiplied by 51.715), V_C is the flow rate of the carrier gas in cm3/min., and 22,400 is the cm^3 per mole at standard temperature and pressure.

Table 1.10: Pre-deposition sources

Dopant	Dopant source	Formula	Usable concentration range	Temperature of source during deposition	State at room temperature
As	Arsine	AsH_3	High	Room temp	Gas
	Arsenic trioxide	As_2O_3	High	200 to 400°C	Solid
	Spin-on		Medium	Room temp	Liquid
	Discs		Low to high	850 to 1,200°C	Solid
B	Boron tribromide	BBr_3	Low to high	10 to 30°C	Liquid
	Boron trichloride	BCl_3	Low to high	Room temp	Gas
	Diborane	B_2H_6	Low to high	Room temp	Gas
	Spin-on		Low to high	Room temp	Liquid
	Boron nitride		Low to high	850 to 1,200°C	Solid
P	Phosphorus pentoxide	P_2O_5	Very high	200 to 300°C	Solid
	Phosphorus Oxychloride	$POCl_3$	Low to high	2 to 40°C	Liquid
	Phosphorus tribromide	PBr_3	Low to high	170°C	Liquid
	Phosphine	PH_3	Low to high	Room temp	Gas
	Spin-on		Low to high	Room temp	Liquid
	Discs		Low to high	Low to high	Solid

Figures 1.39 presents the vapor pressure curves for boron tribromide, phosphorus oxychloride and phosphorus tribromide.

From equations 1.117 and 1.118 and the data presented in figure 1.39 the appropriate conditions for pre-deposition can be calculated.

The preliminary deposition reaction for phosphorus oxychloride is

$$4POCl_3 + 3O_2 \rightarrow 2P_2O_5 + 6Cl_2 \tag{1.119}$$

and the preliminary deposition reaction for boron tribromide is

$$4BBr_3 + 3O_2 \rightarrow 2B_2O_5 + 6Br_2 \tag{1.120}$$

In both reactions a glass layer is formed on the wafer surface and a volatile gas product is produced. Both chlorine and bromine gas can etch silicon if sufficient oxygen is not present. The oxygen causes oxide to grow on the wafer surface both incorporating phosphorus or boron

and liberating phosphorus or boron to diffuse into the wafer. Following pre-deposition the wafer surface is covered with a highly doped glass layer that must be removed by a hydrofluoric acid based de-glaze prior to drive-in. During pre-deposition the inside of the furnace tube is also coated with dopant containing glass. Furnace tubes will typically be saturated with dopant prior to use for pre-depositions as saturating the tube helps to insure that the dopant is present at the silicon surface in quantities high enough to insure the silicon is doped to solid solubility.

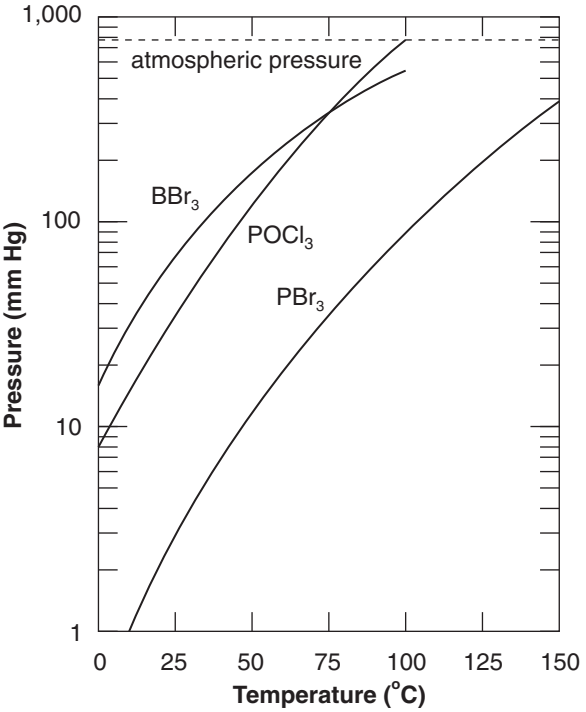

Figure 1.39: Vapor pressure curves for liquid pre-deposition sources [62].

The equations for pre-deposition presented in section 1.6.1 assume that the surface of the semiconductor is at some concentration C_S at time zero. In practice the dopant must be transported to the semiconductor surface and diffuse into the semiconductor before the initial condition is met. The time to reach the initial surface doping level is approximately 1.2 minutes which for short deposition times can be significant [5]. It can be shown that the solution accounting for the initial transport period is [5].

$$\frac{C(x,t)}{C_S} = erf\,\frac{x}{2\sqrt{Dt}} + e^{[ht/\sqrt{Dt}]^2} e^{(ht/\sqrt{Dt})(x2/\sqrt{Dt})} erfc\left[\frac{ht}{\sqrt{Dt}} + \frac{x}{2\sqrt{Dt}}\right] \tag{1.121}$$

where

$$h = h_G/HkT \tag{1.122}$$

and, h_G is the gas phase mass transfer coefficient.

For

$$ht/\sqrt{Dt} > 10 \tag{1.123}$$

equation 1.121 converges to a simple error function.

1.8.9. Redistribution of impurities during epitaxial growth

Bipolar and BiCMOS technologies frequently employ a buried layers, i.e. diffused regions are formed in the substrate followed by epitaxial layer growth (epitaxial layer growth is discussed in chapter 10). During the high temperature epitaxial growth, the impurities diffuse up from the substrate into the epitaxial film. Figure 1.40 schematically illustrates impurity redistribution during epitaxial growth.

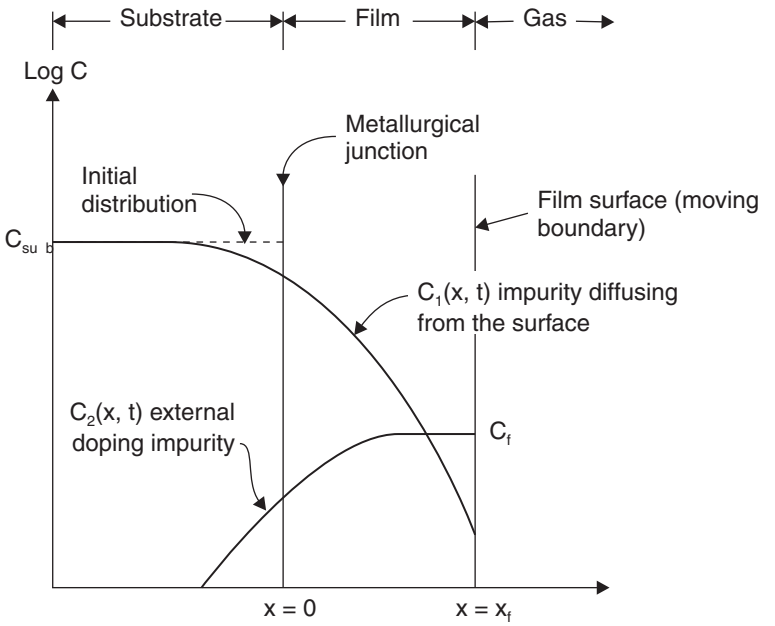

Figure 1.40: Impurity redistribution during epitaxial growth [5].

The solution is [5]

$$\frac{C_1(x,t)}{C_{sub}} = f_1\left[\frac{x}{2\sqrt{Dt}}, \frac{ht}{\sqrt{Dt}}, \frac{Vt}{\sqrt{Dt}}\right] \tag{1.124}$$

where, V is the film growth rate.
For

$$Vt/\sqrt{Dt} \gg 1 \tag{1.125}$$

equation 1.124 reduces to

$$\frac{C_1(x,t)}{C_{sub}} = \frac{1}{2}\, erfc\, \frac{x}{2\sqrt{Dt}} \tag{1.126}$$

regardless of the value of h.

The solution to the external impurity profile is given by

$$\frac{C_2(x,t)}{C_f} = f_2\left[\frac{x}{2\sqrt{Dt}}, \frac{Vt}{\sqrt{Dt}}\right] \tag{1.127}$$

For

$$Vt/\sqrt{Dt} \gg 1 \quad and \quad x \gg 2\sqrt{Dt} \tag{1.128}$$

then equation 1.127 can be approximated by

$$C_2(x,t) = C_f \tag{1.129}$$

and the combined solution for the net impurity level is given by

$$C(x,t) = C_1(x,t) \mp C_2(x,t) \tag{1.130}$$

where the positive sign is used for impurities of the same type and the minus sign is used for impurities of opposite type.

1.8.10. Diffusion in an electric field

The preceding derivations of Fick's law assumed that diffusivity is independent of concentration and that thermal energy is the only driving force for diffusion under the conditions of interest. In fact diffusing charged dopants atoms can be influenced by electric fields in the silicon.

A charged particle in an electric field experiences a force F, given by

$$F = qE \tag{1.131}$$

where, q is the charge on the particle and E is the electric field acting on the particle.

A particle of mass, m, undergoes an acceleration

$$\frac{dv}{dt} = \frac{qE}{m} \tag{1.132}$$

where, v is velocity.

In a solid, the accelerating atom will quickly encounter another atom and undergo elastic scattering randomizing the direction of motion. Scattering can be represented as a restraining force F_r, given by [3]

$$F_r = m\alpha v \tag{1.133}$$

where, α is a proportionality factor related to the collision frequency (collisions/sec.). This gives

$$\frac{dv}{dt} = \frac{1}{m}(F - F_r) = \frac{qE}{m} - \alpha v \tag{1.134}$$

setting dv/dt = 0, the steady state or drift velocity, $-v_d$, can be calculated as

$$v_d = \frac{qE}{m\alpha} \tag{1.135}$$

The mobility μ is defined as

$$\mu \equiv \frac{q}{m\alpha} \tag{1.136}$$

and therefore, combining equations 1.135 and 1.136, yields

$$v_d = \mu E \tag{1.137}$$

The flux j_d due to the uniform motion of impurity atoms is the velocity multiplied by the density, so

$$j_d = \mu CE \tag{1.138}$$

and j_d represents the flux due to diffusion induced by the electric field. Combining the flux due to the concentration gradient - equation 1.12 with the flux due to the electric field - equation 1.139 results in the total flux

$$j_{tot} = -D\frac{\partial C}{\partial x} + \mu CE \tag{1.139}$$

1.9. Diffusion Equipment

Generally, diffusion is accomplished in resistance heated furnaces covered elsewhere in the original book and not repeated here. Arguably some diffusion also occurs in rapid thermal processors - at least unintentionally.

1.10. Metrology

In this section the metrology techniques suitable for diffusion characterization are briefly reviewed. Table 1.11 summarizes some of the more commonly used techniques.

1.10.1. Bevel and Stain

Bevel and stain is a simple, easy to perform technique used to determine junction depth. Either a cylindrical grinding wheel is used to create a groove through the junction to be measured or an angled bevel is ground through the junction. A stain solution is then applied which stains the diffused junction. By knowing the bevel angle or grinding wheel diameter the junction depth may be calculated by measuring the width of the stained area (see figure 1.41).

Table 1.11: Diffusion metrology techniques

Technique	Sensitivity (atoms/cm^3)	Spot size (μm)	Quantity measured
Bevel and stain	~10^{12}	~1mm	Junction depth
Capacitance voltage plotting (CV)	~10^{12}	~0.5mm	Electrically active dopant levels versus depth
Four point probe	~10^{12}	~0.5mm	Sheet resistance - can be converted to average resistivity if the junction depth is known
Secondary ion mass spectroscopy (SIMS)	~10^{16}	~1μm	Atomic concentration and type - can depth profile
Spreading resistance probe (SRP)	~10^{12}	0.1mm	Electrically active dopant versus depth

The junction depth is calculated by measuring x and applying the appropriate geometry corrections to determine x_j.

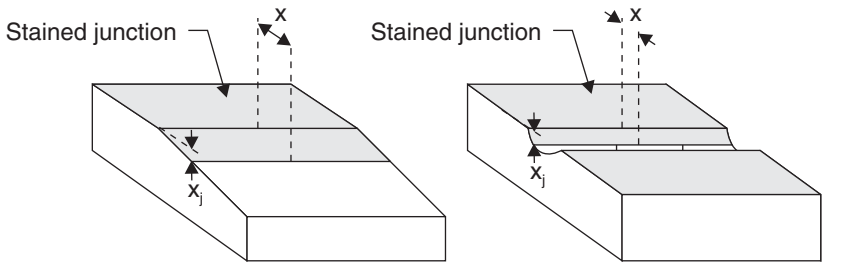

(a) Bevel and stain **(b) Groove and stain**

Figure 1.41: Bevel and stain and groove and stain junction depth measurements.

1.10.2. Capacitance voltage plotting (CV)

The reverse bias capacitance of a pn junction can be utilized to measure impurity levels. The technique requires that a shallow highly doped junction be formed above the impurity profile to be measured. The highly doped junction must be of opposite conductivity type to the impurity being measured (n+ on p or p+ on n). The voltage on the junction is ramped and the instantaneous capacitance is measured. The capacitance can be converted to electrically active impurity concentration by [64]

$$C(V) = \left[\frac{q\varepsilon_S C_B}{2}\right]^{1/2}\left[V_0 \pm \left(V_R - \frac{2kT}{q}\right)\right]^{1/2} \tag{1.140}$$

where, ϵ_S is the permittivity of silicon, C_B is the background concentration, V_0 is the junction potential, and V_R is the reverse bias on the junction.

The limitations to the technique are, the diffusion being measured must be deeper than the shallow diffusion used for measurement plus the zero bias depletion width.

More commonly this technique is applied on an MOS capacitor structure removing the shallow junction restrictions.

1.10.3. Four Point Probe (FPP)

The four-point-probe technique is utilized to measures the sheet resistance of a diffused junction. The FPP technique is illustrated in figure 1.42.

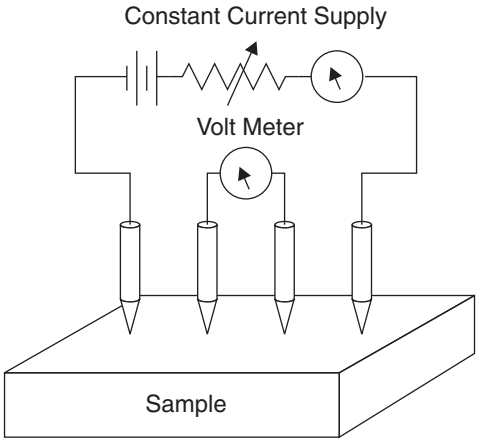

Figure 1.42: Four point probe - sheet resistance measurement system.

In the system illustrated in figure 1.42 a constant current is supplied to the outer two probes and the voltage drop is measured across the inner two probes. The sheet resistance is given by

$$\bar{\rho} = \frac{\pi}{\ln 2}\frac{V}{I}x_j = 4.532\frac{V}{I}x_j = R_S x_j \tag{1.141}$$

where, I is a forced current, V is the measured voltage drop and R_S is the sheet resistance.

For a diffused junction the concentration varies with depth so the average resistivity is given by

$$\bar{\rho} = \frac{x_j}{q}\int_0^{x_j}\frac{1}{C(x)\mu(x)}dx \tag{1.142}$$

where, q is the charge on an electron and $\mu(x)$ is the mobility.Equation 1.142 can be numerically evaluated for diffused gaussian and error function profiles with varying background concentrations. The resulting curves of surface concentration versus average resistivity are known as Irvin curves after the first researcher to present the technique [51].

Figure 1.43 through 1.46 present Irvin curves numerically evaluated by the author utilizing the mobility equations recommended by NIST.

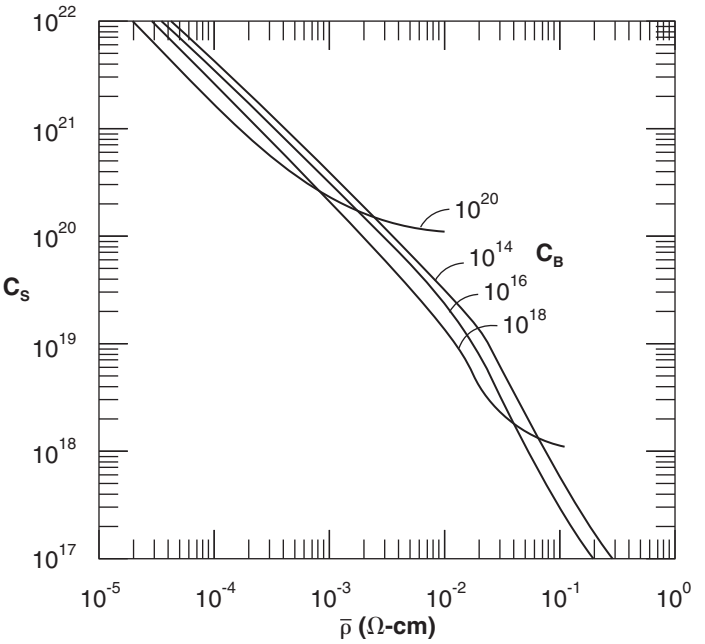

Figure 1.43: Surface concentration versus average resistivity - n type - erfc profile.

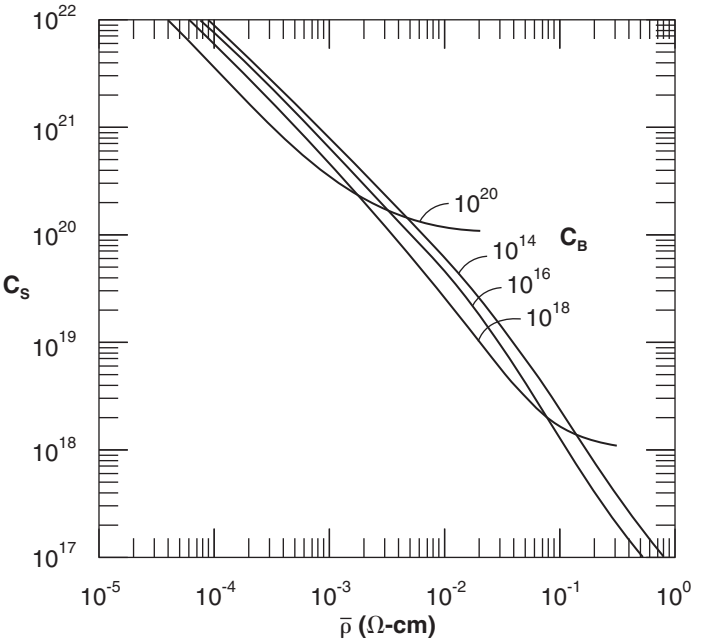

Figure 1.44: Surface concentration versus average resistivity - p type - erfc profile.

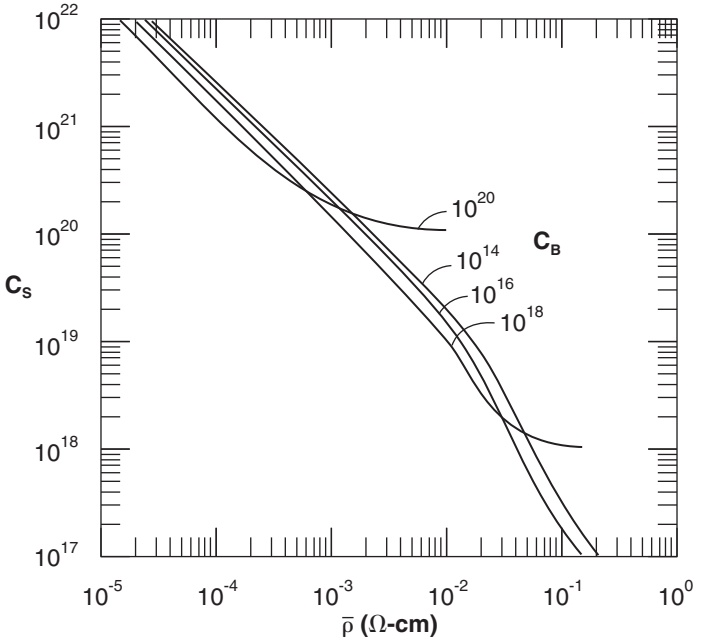

Figure 1.45: Surface concentration versus average resistivity - n type - gaussian profile.

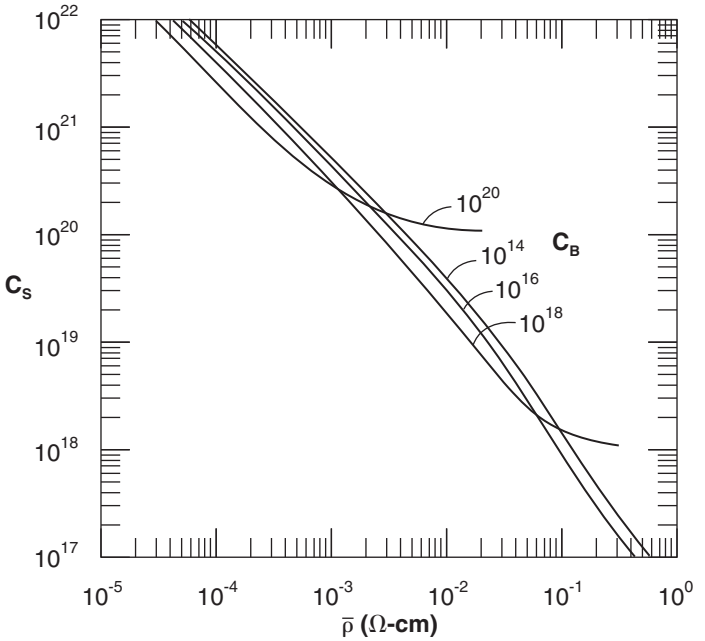

Figure 1.46: Surface concentration versus average resistivity - p type - gaussian profile.

1.10.4. Secondary Ion Mass Spectroscopy (SIMS)

SIMS bombards the section of the wafer to be analyzed with a beam of energetic inert ions. The ion beam sputters ions from the wafer surface that may be mass analyzed to determine the atomic composition.

Continuous bombardment of a surface by the ion beam results in etching so that a depth profile may be determined. The minimum spot size for SIMS is relatively small at 1μm. The drawbacks to SIMS are relatively low sensitivity - approximately 5 x 10^{16} atoms/cm^3, the equipment is expensive and difficult to use - only the largest semiconductor companies can have the technique in-house, and SIMS is destructive. SIMS does however provide atomic concentration versus depth and allow atomic species to be identified. Because of SIMS unique abilities the technique is widely used to analyze doping profile and also to look for contamination.

1.10.5. Spreading Resistance Probe

To perform an SRP analysis the wafer is first bevel ground and polished along a shallow angle. A tiny set of conductive needles are dragged along the beveled surface - see figure 1.47.

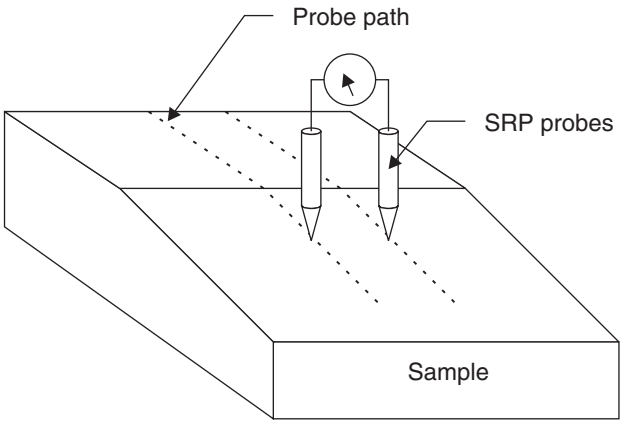

Figure 1.47: Spreading resistance probe analysis.

The needles have a known current applied and the voltage drop across the needles is measured. The resistivity in a small volume under the needle is given by

$$\rho = 2R_{SR}a \tag{1.143}$$

where, R_{SR} is the spreading resistance value and a is a geometric factor determined by measuring a sample of known resistivity.

From the relationship between concentration and resistivity presented in chapter 1 the carrier concentration can be calculated. If the motion of the probes across the bevel is well controlled and the bevel angle is known, the profile versus depth can be calculated. SRP has a couple of limitations, one, only the electrically active dopant is measured so dopants must be activated prior to SRP (this is in contrast to SIMS that measures atomic concentration regard-

less of electronic state), secondly, SRPs require a fairly large measurement area, and third SRP is destructive and very technique sensitive. Most smaller semiconductor companies send out for SRP adding longer turn-around time to the draw backs.

References

[1] W. Scott Ruska, *"Microelectronic Processing - An Introduction to the Manufacture of Integrated Circuits,"* McGraw-Hill Inc. (1987).

[2] Sorab K. Ghandhi, *"VLSI Fabrication Principle: Silicon and Gallium Arsenide,"* John Wiley, (1983).

[3] Sorab K. Ghandhi, *"The Theory and Practice of Microelectronics,"* John Wiley, (1968).

[4] J. Crank, *"The Mathematics of Diffusion,"* Oxford University Press, (1956).

[5] A.S. Grove, *"Physics and Technology of Semiconductor Devices,"* John Wiley (1967).

[6] R.B. Fair, *"Concentration Profiles of Diffuse Dopants in Silicon," in F.Y.Y. Yang, Ed. "Impurity Dopant Processes in Silicon,"* North Holland (1981).

[7] R.B. Fair, *"Diffusion and Ion Implantation," in Gary E. McGuire Ed. "Semiconductor Materials and Process Technology,"* Noyes Publications (1988).

[8] R.B. Fair, J. Appl. Phys., 51, 5828 (1980).

[9] D.A. Antoniadis and I. Moskowitz, J. Appl. Phys., 53, 9214 (1982).

[10] S. Matumoto, Y Ishikawa and T. Niimi, J. Appl. Phys. (1983).

[11] U. Goesle, T.Y. Tan, *"Defects in Semiconductors II,"* S. Mahajan and J.W Corbett Ed. North-Holland Press (1983).

[12] D. Mathiot and J.C. Pfister, J. Appl. Phys., 55, 3518 (1984).

[13] Taniguchi, et.al.

[14] A.M. Lin, R.W. Dutton, and D.A. Antoniadis, Paper 133 presented at the Electrochemical Society Meeting, Boston, Massachusetts, May 6-11 (1979).

[15] Fahey and Dutton.

[16] R.B. Fair and J.C.C. Tsai, J. Electrochem. Soc., 124, 1107 (1977).

[17] P. Fahey, R.W. Dutton and S.M. Hu, Appl. Phys. Lett., 44, 777 (1984).

[18] R.M. Harris and D.A. Antoniadis, Appl. Phys. Lett., 43, 937 (1983).

[19] E. Guerrero, Ph.D. Thesis, University of Vienna (1984).

[20] U. Gosele and T.Y. Tan, *"The Influence of Point Defects on Diffusion and Gettering in Silicon,"* Mat. Res. Soc. Symp. Proc. Vol. 36 (1985).

[21] R.B. Fair, *"The Effect of Strain-Induced Bandgap Narrowing on High Concentration Phosphorus in Silicon,"* J. Appl. Phys., 50, 860 (1979).

[22] Yoshiaki Shibata, Seiichi Hashimoto, Kenji Taniguchi and Chihiro Hamaguchi, *"Oxidation Enhanced Diffusion of Phosphorus over a Wide Range of Oxidation Rates,"* J. Electrochem. Soc. 139, 231 (1992).

[23] B.L. Sharma, *"Diffusion in Semiconductors,"* Trans. Tech. Pub. Germany, 87 (1970).

[24] W. Wurker, K. Roy, and J. Hesse, *"Diffusion and Solid Solubility of Chromium in Silicon,"* Mater. Res. Bull. (U.S.A.), 9, 971 (1974).

[25] H. Kitagano and K. Hashimoto, *"Diffusion Coefficient of Cobalt in Silicon,"* J. Appl. Phys. Jpn., 16, 173 (1977).

[26] J.C. Mikkelsen, Jr., *"Diffusivity of Oxygen in Silicon During Steam Oxidation,"* J. Appl. Phys. Jpn., 16, 173 (1977).

[27] R.F. Bailey and T.G. Mills, *"Diffusion Parameters of Platinum in Silicon,"* in R.R. Habarecht and E.L. Kern, Eds., Semiconductor Silicon 1969, Electrochem. Soc., (1969).

[28] D.L. Kendall and D.B. DeVries, *"Diffusion in Silicon,"* ibid.

[29] V.E. Borisenko, L.F.Gorskaya, A.G. Dutov and V.A. Samuilov, *"Povedenie implantirovannogo fosfora v polikristallicheskom kremnii pri impulsnoii termoobrabotke,"* Electktronnaya Tekhnika, Ser. 2, Poluprovodnikovie Pribori 2, 53 (1987).

[30] M. Takai, M. Izumi, K. Matnunga, K. gamo, S. Namba, T. Minamisono, M. Miyauchi, and T. Hirao, *"Backscattering study of implanted arsenic distribution in poly-silicon on insulator,"* Nucl. Instrum. Methods Phys. Res. B 19/20(1), 603 (1987).

[31] M. Takai, M. Izumi, T. Yamamoto, S. Namba, and T. Minamisono, *"Rapid thermal annealing of arsenic-implanted poly-Si layers on insulator,"* Nucl. Instrum. Methods Phys. Res. B 39(1-4), 352 (1989).

[32] A.D. Buonaquisti, W. Carter, and P.H. Holloway, *"Diffusion characteristics of boron and phosphorus in polycrystalline silicon,"* Thin Solid Films, 100(3), 235 (1983).

[33] T.I. Kamins, J. Manolin, and R.N. Tucker, *"Diffusion of impurities in polycrystalline silicon,"* J. Appl. Phys., 43(1), 83 (1972).

[34] H. Bomgart, H.J. Leamy, G.K. Cellar, and L.E. Trimble, *"Grain boundary diffusion in polycrystalline silicon film on SiO_2,"* J. Phys. (Paris) 43(10), c1/363 (1982).

[35] D.L. Losee, J.P. Lavine, E.A. Trabka, S.T. Lee, and C.M. Jarman, *"Phosphorus diffusion in polycrystalline silicon,"* J. Appl. Phys., 55(4), 1218 (1984).

[36] H. Ryssel, H. Iberl, M. Bleier, G. Prinke, K. Haberger, and H. Kranz, *"Arsenic - implanted polysilicon layers,"* Appl. Phys. 24(3), 197 (1981).

[37] B. Swaminathan, K.C. Saraswat, R.W. Dutton, and T.I. Kamins, *"Diffusion of arsenic in polycrystalline silicon,"* J. Appl. Phys. Lett., 40(9), 795 (1982).

[38] M. Arienzo, Y. Komen, and A.E. Michel, *"Diffusion of arsenic in bilayer polycrystalline silicon films,"* J. Appl. Phys., 55(2), 365 (1984).

[39] K. Tsukamoto, Y. Akasaka, and K. Horie, *"Arsenic implantation into polycrystalline silicon and diffusion to silicon substrate,"* J. Appl. Phys. 48(5), 1815 (1977).

[40] F.H.M. Spit, H. Albers, A. Lubbes, Q.J.A. Rijke, L.J. Van Ruijven, J.P.A. Westerveld, H. Bakker, and S. Radelaar, *"Diffusion of antimony (125Sb) in polycrystalline silicon,"* Phys. Status Solidi A, 89(1) 105 (1985).

[41] Victor E. Borisenko and Peter J. Hesketh, *"Rapid Thermal Processing of Semiconductor"* Plenum Press (1997).

[42] M. Ghezzo and D.M. Brown, *"Diffusivity Summary of B, Ga, P, As, and Sb in SiO_2,"* J. Electrochem. Soc., 120, 146 (1973).

[43] Y. Wada and D.A. Antoniadis, *"Anomalous Arsenic Diffusion in Silicon Dioxide,"* J. Electrochem. Soc., 128, 1317 (1981).

[44] J.C.C. Tsai, *"Diffusion,"* S.M. Sze Ed. *"VLSI Technology,"* McGraw Hill (1983).

[45] R.N. Ghoshtagore, *"Silicon Dioxide Masking of Phosphorus Diffusion in Silicon,"* Solid State Electron., 18, 399 (1975).

[46] C.Y. Bartholomew "private communications" as reported in J.C.C. Tsai, *"Diffusion,"* W.E. Beadle, J.C.C. Tsai and R.D. Plummer Eds. *"Quick Reference Manual for Silicon Integrated Circuit Technology,"* John Wiley (1985).

[47] F.A. Trumbore, *"Solid solubilities of impurity elements in germanium and silicon,"*, Bell Syst. tech. J., 39, 205 (1960).

[48] V.E. Borisenko and S.G. Yudin, *"Steady-state solubility of substitutional impurities in silicon,"* Phys. Status Solidi, A 101(1) 123 (1987).

[49] M.Y. Tsai, F.F. Morehead, and J.E.E. Baglin, *"Shallow Junctions by High Dose As Implants in Si: Experiments and Modeling,"* J. Appl. Phys., 51, 3230 (1980).

[50] E. Guerrero, H. Potzl, R. Tielert, M. Grasserbauer, and G. Stingeder, *"Generalized Model for the Clustering of As Dopant in Si,"* J. Electrochem. Soc., 129, 1826 (1982).

[51] J.C. Irvin, *"Resistivity of Bulk Silicon and of Diffused Layers in Silicon,"* Bell System Tech. J., 41, 387 (1962).

[52] D.P. Kennedy and R.R. O'Brien, *"Analysis of the Impurity Atom Distribution Near the Diffusion Mask for a Planar p-n Junction,"* IBM J. Res. Dev., 9(3), 179 (1965).

[53] C.T. Shaw, H. Sello, and D.A. Tremere, *"Diffusion of Phosphorus in Silicon Dioxide Film,"* J. Phys. Chem. Solids, 11, 288 (1959).

[54] O.D. Trapp, *"Semiconductor Technology Handbook,"* Technology Associates (1993).

[55] M.M. Atalla and E. Tannenbaum, *"Impurity Redistribution and Junction Formation in Silicon by Thermal Oxidation,"* Bell System Tech. J., 39, 933 (1960).

[56] A.S. Grove, O.Leistiko, and C.T. Sah, *"Redistribution of Acceptor and Donor Impurities During Thermal Oxidation of Silicon,"* J. Appl. Phys., 35, 2695 (1964).

[57] J.W. Colby and L.E. Katz, *"Boron Segregation at Si-SiO_2 Interface as a function of Temperature and Orientation,"* J. Electrochem. Soc., 123, 409 (1976).

[58] R.B. Fair and J.C.C. Tsai, J. Electrochem. Soc. 122, 1689 (1975).

[59] K. Sakamoto, K. Nishi, F. Ichikawa and S. Ushio, *"Segregation and transport coefficients of impurities at the Si/SiO_2 interface,"* J. Appl. Phys., 61, 1553 (1987).

[60] B.E. Grove, A.S. Grove, E.H. Snow, and C.T. Sah, *"Observation of Impurity Redistribution During Thermal Oxidation of Silicon Using the MOS Structure,"* J. Electrochem. Soc., 112, 308 (1965).

[61] J.C.C. Tsai, *"Diffusion,"* W.E. beadle, J.C.C. Tsai and R.D. Plummer, Eds. *"Quick Reference Manual for Silicon Integrated Circuit Technology,"* John Wiley (1985).

[62] J.C. Schumacher Company applications notes.

[63] Scotten W. Jones, *"Process technology for the 21st Century,"* Semiconductor Consulting Services (1999).

[64] S. Wolf and R.N. Tauber, *"Silicon processing for the VLSI Era: Volume 1 - Process Technology,"* Lattice Press (1986).

[65] R.L. Burden, J.D. Faires and, A.C. Reynolds, *"Numerical Analysis,"* 2nd ed. Prindle Weber and Schmidt (1981).

[66] Richard B. Fair, *"Unified Model of Boron Diffusion in Thin Gate Oxides: Effects of F, H_2, N, Oxide Thickness and Injected Si Interstitials,"* IEDM 95, 85, (1995).

[67] H.J. Grossman, *"Dopants and Intrinsic Point-Defects During Si Device Processing,"* in H.R. Huff, U. Gosele and H. Tsuya, eds. *"Semiconductor Silicon 1998,"* Electrochem. Soc. Proc., 98-1, (1998).
[68] M.D. Giles, Apld. Phys. Lett., 62, 1940 (1993).
[69] T. Diaz de la Rubia and G.H. Gilmer, Phys. Rev. Lett. 74, 2507 (1995).
[70] James D. Plummer, *"Point Defect Based Modeling of Dopant Diffusion and Transient Enhanced Diffusion in Silicon,"* in H.R. Huff, U. Gosele and H. Tsuya, eds. *"Semiconductor Silicon 1998,"* Electrochem. Soc. Proc., 98-1, (1998).
[71] E. Guerrero, W. Jungling, H. Potzl, U. Gosele, L. Mader, M. Grasserbauer, and G. Stingeder, *"Determination of the Retarded Diffusion of Antimony by SIMS Measurement and Numerical Simulation,"* J. Electrochem. Soc., 133, 2181 (1986).

Example Problems

1. A pre-deposition cycle is desired to produce a phosphorus diffusion with a surface concentration of 2 x 10^{20} atoms/cm^3 and a junction depth of 0.5μms when diffused into a background concentration of 1 x 10^{18} atoms/cm^3.

- From figure 7.25 find the temperature where phosphorous has a solid solubility of 3 x 10^{20} atoms/cm^2 - ~ 900^{o}C.
- To determine the pre-deposition time required to produce a 0.2μm junction depth at the temperature determined in step 1. First divide the background concentration by the surface concentration, 1 x 10^{18}/3 x 10^{20} = 3.3 x 10^{-3}. Next using figure 7.11 find the value of z for an error function that corresponds to 3.3 x 10^{-3}, ~2.15. Convert z to the required Dt, $(x/2z)^2$ = Dt -> 2.16 x 10^{-11} cm^2. Find the diffusivity of phosphorus for 900^{o}C (this is complicated by the concentration dependence of phosphorus diffusivity, for simplicity assume 5 x 10^{19} as an average concentration). From figure 7.18 the diffusivity is ~2 x 10^{-15}. Dividing 2.16 x 10^{-11} by 2 x 10^{-15} gives 10,817 secs or ~180mins.
- To determine the oxide thickness required to mask against a 180min phosphorus pre-deposition at 900^{o}C, from figure 7.37, ~0.3μms.

2. A drive-in cycle is desired to produce a surface concentration of 1 x 10^{18} and a junction depth of 1μm when diffused into a background concentration of 1 x 10^{14}.

- To determine the required Dt, divide the background concentration by the surface concentration, 1 x 10^{14}/ 1 x 10^{18} -> 1 x 10^{-4}. Look up z for a gaussian profile for 1 x 10^{-4}, from figure 7.11, ~3.1. Converting z to Dt (see above) gives 2.6 x 10^{-10}. Using figure 7.15 for the intrinsic diffusivity of boron the time and temperature can be contrasted to produce an acceptable cycle length, ~1,060 gives a diffusivity of ~5 x 10^{-14} and a cycle time of ~87mins.
- To determine the required pre-deposition doping level for a 1 x 10^{18} surface concentration after a Dt of 2.6 x 10^{-10}. Rearranging equation 7.40 gives $C_S(\pi Dt)^{1/2} = Q$ -> 2.86 x 10^{13}.

Problems

1. Calculate a pre-deposition cycle to produce a boron diffusion with a surface concentration of 1 x 10^{18} atoms/cm3, and a junction depth of 0.5μms into a background concentration of 1 x 10^{14} atoms/cm^3.
2. Calculate the junction depth for the pre-deposition calculated in 1) following a 5 hour diffusion at 1,050°C in N_2.
3. Calculate the junction depth for the pre-deposition calculated in 1) following a 5 hour diffusion at 1,050°C in dry O_2.
4. Calculate the surface concentration of boron under the conditions outlined in 1) and in 2). Describe why the surface concentration is different.
5. Calculate the minimum carrier gas flow rate for BBr_3 to meet the pre-deposition conditions outline in 1).
6. Calculate the lateral diffusion of a junction formed under the conditions outlined in 2).
7. Calculate the effective Dt for an arsenic diffusion ramped from 750°C to 1,050°C at 5°C/min.

Appendix

Properties of the error function

$$erf(x) \equiv \frac{2}{\sqrt{\pi}} \int_0^{\infty} e^{-a^2} da = \frac{2}{\sqrt{\pi}} \left[x - \frac{x^3}{3 \cdot 1!} + \frac{x^5}{5 \cdot 2!} - \frac{x^7}{7 \cdot 3!} + \ldots \right] \tag{F.1}$$

$$erfc(x) \equiv 1 - erf(x) \tag{F.2}$$

$$erf(0) = 0 \tag{F.3}$$

$$erf(\infty) = 1 \tag{F.4}$$

$$erf(x) \cong \frac{2}{\sqrt{\pi}} x \quad \text{for x << 1} \tag{F.5}$$

$$erfc(x) \cong \frac{1}{\sqrt{\pi}} \frac{e^{-x^2}}{x} \quad \text{for x >> 1} \tag{F.6}$$

$$\frac{d\ erf(x)}{dx} = \frac{2}{\sqrt{\pi}} e^{-x^2} \tag{F.7}$$

$$\int_0^{\infty} erfc(x')dx' = x\ erfc\ x + \frac{1}{\sqrt{\pi}}(1 - e^{-x^2}) \tag{F.8}$$

$$\int_0^{\infty} erfc(x)dx = \frac{1}{\sqrt{\pi}} \tag{F.9}$$

Table E.1: Values of the complementary error function (erfc)

z	erfc(z)	z	erfc(z)	z	erfc(z)
0.0	1.00000000	1.3	0.06599207	2.6	0.00023603
0.1	0.88753708	1.4	0.04771489	2.7	0.00013433
0.2	0.77729741	1.5	0.03389486	2.8	0.00007501
0.3	0.67137324	1.6	0.02365162	2.9	0.00004110
0.4	0.57160765	1.7	0.01620954	3.0	0.00002209
0.5	0.47950012	1.8	0.01090950	3.1	0.00001165
0.6	0.39614391	1.9	0.00720957	3.2	0.00000603
0.7	0.32219881	2.0	0.00467774	3.3	0.00000306
0.8	0.25789921	2.1	0.00297947	3.4	0.00000152
0.9	0.20309189	2.2	0.00186285	3.5	0.00000074
1.0	0.15729926	2.3	0.00114318	3.6	0.00000036
1.1	0.11979496	2.4	0.00068851	3.7	0.00000017
1.2	0.08968604	2.5	0.00040695	3.8	0.00000008